Two types of non-selective cation channel opened by muscarinic stimulation with carbachol in bovine ciliary muscle cells

Yoshiko Takai[1], Ryoichi Sugawara[1], Hiroshi Ohinata[2] and Akira Takai[2]

Departments of [1]Ophthalmology and [2]Physiology, Asahikawa Medical College, Asahikawa 078-8510, Hokkaido, Japan

In the ciliary muscle, the tonic contraction requires a sustained influx of Ca^{2+} through the cell membrane. However, little has hitherto been known about the route(s) of Ca^{2+} influx in this tissue that lacks voltage-gated Ca^{2+} channels. To identify ion channels as the Ca^{2+} entry pathway we studied the effects of carbachol (CCh) on freshly isolated bovine ciliary muscle cells by whole-cell voltage clamp. Experiments were carried out using pipettes filled with K^+-free solution containing 100 mM caesium aspartate, 5 mM BAPTA and 180 μM GTP (pH 7.0; the intracellular free Ca^{2+} concentration, $[Ca^{2+}]_i = 70$ nM). CCh evoked an inward current showing polarity reversal at a holding potential near 0 mV. Analysis of the current noise distinguished two types of non-selective cation channel (NSCCL and NSCCS) with widely different unitary conductances (35 pS and 100 fS). The ratios of the permeabilities to Li^+, Na^+, Cs^+, Mg^{2+}, Ca^{2+}, Sr^{2+} and Ba^{2+}, estimated by cation replacement procedures, were 0.9 : 1.0 : 1.5 : 0.2 : 0.3 : 0.4 : 0.5 for NSCCL, and 1.0 : 1.0 : 1.8 : 2.5 : 2.6 : 3.2 : 5.0 for NSCCS. NSCCS, but not NSCCL, was strongly inhibited by elevation of $[Ca^{2+}]_i$. Both NSCCL and NSCCS were dose-dependently inhibited by 1–100 μM SKF96365, La^{3+} and Gd^{3+}, which also inhibited the tonic component of the contraction produced in muscle bundles by CCh without markedly affecting the initial phasic component. NSCCL and/or NSCCS may serve as a major Ca^{2+} entry pathway required for sustained contraction of the bovine ciliary muscle. RT-PCR experiments in the bovine ciliary muscle (whole tissue) detected mRNAs of several transient receptor potential (TRP) channel homologues (TRPC1, TRPC3, TRPC4 and TRPC6), which are now regarded as possible molecular candidates for receptor-operated cation channels.

(Received 1 April 2004; accepted after revision 15 July 2004; first published online 22 July 2004)

Corresponding author A. Takai: Department of Physiology, Asahikawa Medical College, Asahikawa 078-8510, Hokkaido, Japan. Email: takai@asahikawa-med.ac.jp

The ciliary muscle, an intraocular muscle responsible for visual accommodation and regulation of aqueous humour outflow, is densely innervated by cholinergic nerve fibres, and its contraction is initiated and sustained by stimulation of muscarinic receptors on the surface of the muscle cell membrane by the transmitter acetylcholine (Glasser & Kaufman, 2003). In many other mammalian smooth muscles, contraction induced by muscarinic stimulation has long been known to be accompanied by a depolarization concomitant with an increase in the conductance of the cell membrane, and this is usually attributed to the opening of cation channels with low ion selectivity, termed 'receptor-operated' non-selective cation channels (NSCCs) (Bolton, 1979; McFadzean & Gibson, 2002). Depolarization in response to muscarinic stimulation has also been demonstrated by the intracellular microelectrode method in dog ciliary muscle (Ito & Yoshitomi, 1986) and in a human ciliary muscle cell line (Korbmacher *et al.* 1990). In previous experiments we have examined the effects of a cholinergic agonist, carbachol (CCh), on the membrane potential and current in smooth muscle cells freshly isolated from the bovine ciliary body, using the whole-cell clamp method (Takai *et al.* 1997). We have confirmed thereby that, under current clamp at 0 pA, CCh causes an atropine-sensitive depolarizing response which is concurrent with an increase in the membrane conductance. We have also shown that, under voltage clamp, CCh evokes a current which is resistant to organic Ca^{2+} channel antagonists and reverses the polarity at a holding potential near 0 mV (Takai *et al.* 1997). These previous observations strongly suggest that muscarinic

 DOI: 10.1113/jphysiol.2004.065607

stimulants activate some type(s) of NSCC to produce the electrical phenomena in the ciliary muscle.

However, our knowledge about the channels in the ciliary muscle is still very limited. For example, no experimental evidence has hitherto been available to determine whether muscarinic stimulation activates a single species of NSCC or more than one type of NSCC. Although the polarity reversal at a potential near 0 mV is indicative of a low ion selectivity, quantitative comparison of the relative permeabilities of the channels to cations has not been performed. Also, very little is known about the functional roles for the channels. Even if the opening of the channels causes a depolarization of the muscle cell membrane, it has been shown that depolarization by itself cannot initiate or maintain the contraction of the ciliary muscle (Suzuki, 1983).

In the present experiments, as a continuation of our previous study on the bovine ciliary muscle, we have further examined the properties of the currents evoked by superfusion of CCh under whole-cell voltage clamp. Since transient receptor potential (TRP) channel homologues are now considered as possible molecular candidates for receptor-operated NSCCs (see Clapham *et al.* 2001; Minke & Cook, 2002; Inoue *et al.* 2003), we have also examined the existence of their mRNAs in the ciliary muscle by RT-PCR. By analysing the noise of the currents evoked by CCh we have obtained results that indicate that, in most ciliary muscle cells, muscarinic stimulation activates two types of NSCC (NSCCL and NSCCS) with widely different single-channel conductances (35 pS and 100 fS). These channels differ from each other with regard to the activation kinetics as well as in the relative permeabilities to alkali and alkaline earth metal ions, and are likely to be linked to muscarinic receptors by different signalling pathways. We also show that several substances that inhibit the CCh-evoked NSCC currents also inhibit the tonic component of the contraction of ciliary muscle bundles induced by CCh without strongly affecting the initial phasic component. NSCCL and/or NSCCS, either of which admits Ca^{2+}, may act as a pathway for Ca^{2+} entry required for sustained contraction of the ciliary smooth muscle. In the RT-PCR experiments we have detected at least four types (TRPC1, TRPC3, TRPC4 and TRPC6) of TRP mRNA in the bovine ciliary muscle.

Methods

Solutions and chemicals

The normal physiological saline solution (PSS) used was of the following composition (mM): NaCl, 127; KCl, 5.9; $CaCl_2$, 2.4; $MgCl_2$, 1.2; glucose, 11.8; Hepes, 10. The pH was adjusted to 7.4 (at 30°C) by titration with NaOH. In the cation substitution experiments, NaCl, KCl, $CaCl_2$ and $MgCl_2$ in PSS were totally replaced with an isosmotic concentration of an alkaline metal salt (LiCl, NaCl or CsCl; 138 mM) or an alkaline earth metal salt ($MgCl_2$, $CaCl_2$, $SrCl_2$ or $BaCl_2$; 92 mM). High K^+ (100 mM) PSS was prepared by replacing NaCl with equimolar KCl.

Unless otherwise mentioned, pipettes for whole-cell clamp experiments were filled with a solution containing (mM): NaCl, 5; caesium aspartate, 100; $MgCl_2$ 5; ATP (disodium salt), 5; Hepes, 20; 1,2-bis (2-aminophenoxy)ethane-*N*,*N*,*N*′,*N*′-tetraacetic acid (BAPTA), 5; and GTP, 0.18. The pH was adjusted to 7.0 with NaOH. The free Ca^{2+} concentration was adjusted by changing the Ca/BAPTA ratio. The apparent dissociation constant of BAPTA for Ca^{2+} was assumed to be 0.35 μM (Takai *et al.* 1997). Pipettes used for on-cell patch clamp experiments were filled with normal PSS.

Carbamylcholine chloride (carbachol; CCh), atropine sulphate, GTP, guanosine 5′-*O*-(3-thiotriphosphate) (GTPγS), pertussis toxin and cholera toxin were purchased from Sigma Chemical Co. (St Louis, MO, USA). BAPTA was obtained from Dojindo Laboratories (Tabaru, Kumamoto, Japan). Iberiotoxin (synthetic) was a product of Peptide Institute, Co. (Osaka, Japan). All other chemicals used were of analytical grade.

Experiments were carried out at 30°C, unless otherwise mentioned.

Preparation of ciliary muscle cells

Bovine eyes were enucleated soon after the animals were killed in a local slaughterhouse and transported to our laboratory in ice-cooled PSS. The eyes were incised circumferentially about 5 mm posterior to the limbus, and after the vitreous humour and lens were removed, the ciliary muscle was carefully dissected out from the scleral spur. Single muscle cells were obtained by the method previously described (Takai *et al.* 1997). Briefly, the excised muscle was equilibrated in nominally Ca^{2+}-free PSS containing 100 mM K^+ at 35°C for 30 min and transferred to a solution of the same composition supplemented with 0.4% (w/v) collagenase (Wako Junyaku Co.) and 0.02% (w/v) papain (Sigma). After incubation for 20–25 min, the cell suspension was filtered with a fine nylon mesh. The dispersed cells were collected by centrifuging at 200 *g* for 2 min and then resuspended in nominally Ca^{2+}-free, high K^+ (100 mM) PSS.

Electrical recordings

An Axopatch 200B amplifier (Axon Instruments, Foster City, CA, USA) was used for voltage clamp experiments. The borosilicate glass pipettes used had a resistance of 13.5 ± 0.3 MΩ ($n = 49$) when filled with the pipette solution for whole-cell voltage clamp. For command pulse generation and digital data acquisition we used a Digidata 1200B interface controlled by the pCLAMP

software (version 9; Axon Instruments) running on a Windows-based computer. Relatively short sections of data were recorded on a magnetoptic disk after on-line digitization. Long sections of data were recorded on a video cassette using an RP-880 PCM converting system (NF Electronic Instruments, Tokyo, Japan). Mathematical processing and analysis of data were carried out using the ClampFit software (version 9; Axon Instruments, Foster City, CA, USA) and the Origin software (version 7.5; OriginLab, Northampton, MA, USA).

Noise analyses

Non-stationary variance analysis. The current signal was filtered by an analog 4-pole Bessel filter at 1 kHz (−3 dB) and digitized at 2 kHz, before the mean μ and the variance σ^2 around the mean were calculated for every 500 sample points.

The unitary current amplitudes were estimated from the slopes of the best-fit lines obtained by linear regression of (μ, σ^2) data, assuming the following relationship (see, e.g. Sigworth, 1980)

$$\sigma^2 = \zeta\mu + {\sigma_0}^2 \tag{1}$$

where ζ denotes the unitary current amplitude and ${\sigma_0}^2$ represents the contributions from undesired fluctuations such as thermal noise in the voltage clamp. For this purpose we selected CCh-evoked responses such that their μ–σ^2 relationships could be fitted by single straight lines (see Fig. 2). The unitary chord conductances were then calculated, using the value of ζ estimated as the slope of the regression line, as

$$\gamma = \frac{\zeta}{E_\mathrm{h} - E_\mathrm{r}} \tag{2}$$

where γ is the unitary conductance, E_h is the holding potential and E_r is the zero-current potential (i.e. the potential of polarity reversal).

Note that the relationship between μ and σ^2 is more generally written

$$\begin{aligned}\sigma^2 &= \zeta\mu - \frac{1}{N}\mu^2 + {\sigma_0}^2 \\ &= \zeta\mu(1-p) + {\sigma_0}^2\end{aligned} \tag{3}$$

where N is the number of the channels and p is the non-stationary open-state probability (Sigworth, 1980). Equation (1) is a limiting case of eqn (3) where $p \to 0$.

Spectral analysis. The signals from the cassette tape were digitized at 5 kHz and digitally high-pass filtered at 0.2 Hz and low-pass filtered at 2 kHz (−3 dB, 8-pole Butterworth). These band-passed noise data were divided into segments each containing 4096 or 8192 data points, for which two-sided power spectral densities were calculated by fast Fourier transform and then averaged to obtain a mean noise power spectrum. The net two-sided spectral density for agonist-induced currents was obtained by subtracting the mean spectrum of noise in the absence of agonist from that in its presence.

The positive-frequency halves of the symmetrical two-sided net spectra were fitted by non-linear least-squares method (Levenberg-Marquardt algorithm) with the model function defined as the sum of two Lorentzian components:

$$S(f) = \frac{S_1(0)}{1 + (f/f_1)^2} + \frac{S_2(0)}{1 + (f/f_2)^2} \tag{4}$$

where $S(f)$ is the two-sided power density at the frequency f, $S_1(0)$ (>0) and $S_2(0)$ (≥ 0) are the zero-frequency asymptotes, and f_1 and f_2 $(0 < f_1 < f_2)$ are the corner frequencies. If all noise components of an agonist-induced current are detected in the frequency domain as the sum of two Lorentzians, then we will have

$${\sigma_\mathrm{c}}^2 \equiv \sigma^2 - {\sigma_0}^2 = \pi f_1 S_1(0) + \pi f_2 S_2(0) \tag{5}$$

where ${\sigma_\mathrm{c}}^2$ denotes the variance of the agonist-induced current in the time domain (Cull-Candy *et al.* 1988; Howe *et al.* 1988).

Some (but not all) power spectra with two Lorentzian components can be simulated using a simple three-state reaction model (Colquhoun & Hawkes, 1977):

$$\mathrm{A} + \mathrm{R} \underset{k_2}{\overset{k_1}{\rightleftharpoons}} \mathrm{AR} \underset{\alpha}{\overset{\beta}{\rightleftharpoons}} \mathrm{AR}^* \qquad \text{Scheme 1}$$

where A is the agonist, and R and R* denote the closed channel and the open channel, respectively, which are complexed with the receptor. Now, assign the molar concentration of the agonist to c and write the spectral function in the form of eqn (4); then, for this particular model, $f_1, f_2, S_1(0)$ and $S_2(0)$ are given as explicit functions of the rate constants, k_1, k_2, α and β, as follows (see Colquhoun & Hawkes, 1977):

$$f_1 = -\lambda_1/2\pi, \tag{6}$$

$$f_2 = -\lambda_2/2\pi, \tag{7}$$

$$S_1(0) = \frac{-2(\lambda_2 + \alpha)\lambda_2\zeta\mu}{(\lambda_2 - \lambda_1)(k_1 c + \lambda_2)\xi\lambda_1} \tag{8}$$

and

$$S_2(0) = \frac{2(\lambda_1 + \alpha)\lambda_1\zeta\mu}{(\lambda_2 - \lambda_1)(k_1 c + \lambda_1)\xi\lambda_2}, \tag{9}$$

where

$$\xi = \frac{k_1}{k_2}\left(1 + \frac{\beta}{\alpha}\right)c + 1,$$

$$\lambda_1 = -\left[\alpha + \beta + k_1 c + k_2 - \sqrt{(\alpha + \beta + k_1 c + k_2)^2 - 4\alpha\xi k_2}\right]/2$$

and

$$\lambda_2 = -\left[\alpha + \beta + k_1 c + k_2 + \sqrt{(\alpha + \beta + k_1 c + k_2)^2 - 4\alpha\xi k_2}\right]/2$$

The equilibrium probabilities, p_{AR^*}, p_{AR} and p_{A+R}, that the channel occupies each of the three states, AR*, AR and A + R, are also explicitly given, as functions of c, by the following set of equations:

$$p_{AR^*} = \frac{k_1\beta c}{k_2\alpha\xi}; \quad p_{AR} = \frac{k_1 c}{k_2\xi}; \quad p_{A+R} = \frac{1}{\xi} \qquad (10)$$

Note that $p_{AR^*} + p_{AR} + p_{A+R} = 1$.

The dose–activation relationship for the agonist is related to p_{AR^*} ($= p_{AR^*}(c)$) by

$$\phi(c) = \frac{p_{AR^*}(c)}{p_{AR^*}(\infty)} = \frac{c}{K + c} \qquad (11)$$

where $\phi(c)$ is the fractional intensity of the response at c, and K is the apparent dissociation constant defined by

$$K = \frac{k_2\alpha}{k_1(\alpha + \beta)} \qquad (12)$$

Obviously, the use of the reaction model (Scheme 1) is justified only when there exists a set of physico-chemically realistic values of k_1, k_2, α and β which gives a reasonable fit of the spectral function to data. In the present experiments we tried to estimate such values by numerically solving the eqns (6)–(9) simultaneously in terms of k_1, k_2, α and β with the use of the values of f_1, f_2, $S_1(0)$ and $S_2(0)$ determined by directly fitting the model function eqn (4) to the spectral data. For this purpose, we used the Mathematica software (version 5.0; Wolfram Research, Champaign, IL, USA). We also tried to fit the spectral data by the non-linear least-squares method with the model function eqn (4) after making the substitutions defined by eqns (6)–(9), and thereby estimate the values of k_1, k_2, α and β.

Permeability ratios

The ratio of the permeability of a monovalent or bivalent cation to that of Na^+ was estimated from the shift of reversal potential caused by total substitution of Na^+, K^+, Ca^{2+} and Mg^{2+} in the bath solution with the cation, using the following equation (Lewis, 1979):

$$\frac{P_X}{P_{Na}} = \frac{[Na^+]_o}{z^2[X]_o} \exp\left\{\frac{F(E_X - E_{Na})}{RT}\right\} \times \left\{1 + \exp\left(\frac{FE_X}{RT}\right)\right\}^{z-1} \qquad (13)$$

where X represents the substitute ion (which may be Na^+ itself), z (= 1 or 2) is the valency of X, $[X]_o$ is the extracellular concentration of X, P_X is the permeability coefficient for X, E_X is the reversal potential measured using X as the substitute, and F, R and T have their usual thermodynamic meanings.

Mechanical recordings

The methods of tension recording and of superfusion were essentially the same as previously described (Ashoori *et al.* 1985). Briefly, a small piece (about 1 mm wide and 5 mm long) of smooth muscle was carefully dissected from an excised ciliary muscle bundle. The preparation was vertically mounted in a small organ bath (0.5 ml in volume) through which solution flowed at a constant rate of 2 ml ml^{-1}. The tension was isometrically recorded using a U-gauge transducer (type UL-2GR; Minebea Co., Tokyo, Japan) and a potentiometric pen-recorder.

RT-PCR experiments

A QuickPrep mRNA purification kit (Amersham Biosciences, Little Chalfont, UK) was used to isolate polyadenylated mRNA from the bovine ciliary muscle (whole tissue; 10–50 mg). The polyadenylated mRNA obtained was transcribed to first-strand cDNA using a PowerScript reverse transcriptase (BD Biosciences, San Jose, CA, USA) and a 5′-d$(T)_{25}N_{-1}$N-3′ primer (where N = A, C, G or T; and N_{-1} = A, G or C). GeneAmp PCR System 9700 thermal cyclers (Applied Biosystems, Foster City, CA, USA) were used to amplify transient receptor potential cannonical (TRPC) sequences with Advantage 2 polymerase (BD Biosciences) and the gene-specific primer pairs (see Table 2) which were designed, based on the reference sequences (see Table 2) obtained from the GenBank database. Either a two-step or a three-step PCR protocol (with 30–45 thermal cycles) was chosen, depending on the theoretical melting temperature for each primer pair. The products of the PCR reactions were immediately subjected to electrophoresis in agarose gel (0.9–1.2%). The gels were stained with SYBR Gold fluorescent dye (Molecular Probes, Eugene, OR, USA) after electrophoresis and visualized with a DarkReader visible light transilluminator (Clare Chemical Research, Dolores, CO, USA). Amplified DNA fragments of expected sizes were routinely extracted from the gel and subcloned into a pCR4-TOPO sequencing vector (Invitrogen). The vector was transformed into chemically competent DH5α *E. coli* cells which were then cultured after colony selection using ampicillin as the marker. The nucleotide sequence of the insert in the plasmid isolated from the culture was analysed by a Long-Read Tower sequencer (Amersham Biosciences) after thermal cycling reaction with Thermo-Sequenase DNA polymerase and CyDye terminators

(Amersham Biosciences). For primer pairs which gave no clear specific amplification in initial trials, we examined the effects of changing the annealing temperature in a $\pm 5^{\circ}$C range around the value suggested by the Oligo software (Molecular Biology Insights, Cascade, CO, USA) using a gradient thermal cycler (MasterCycler Gradient, Eppendorf, Hannover, Germany), and thereby tried to find appropriate amplification conditions.

To evaluate the quality of the first-strand cDNA libraries, we used the GeneChecker primer kit (Invitrogen), a set of five pairs of PCR primers which amplify specific regions of several highly conserved mammalian genes: the glyceraldehyde-3-phosphate dehydrogenase (GAPDH) gene, the 5′ and 3′ ends of the β-actin gene, and the 5′ (6 kb) and 3′ (2 kb) ends of the clathrin gene. Only cDNA libraries for which all these five primer pairs gave a clear specific amplification (see Fig. 13) were used for the PCR analysis of TRPCs.

Analysis of dose–inhibition relationships

To describe dose–response relationships, we generally used the Hill function

$$\phi(x) = \frac{\phi_{\max} x^h}{K^h + x^h} \qquad (14)$$

where $\phi(x)$ is the intensity of the response in the presence of an activator or inhibitor whose concentration is x, $\phi_{\max}$ is the maximal or control response, K denotes the apparent dissociation constant and h stands for the Hill coefficient ($h > 0$ for dose–activation relationships and $h < 0$ for dose–inhibition relationships). Note that eqn (11) is a special form of eqn (14). The values of K and h were estimated with standard errors by fitting this model function to the data by non-linear least squares regression, using as weight the reciprocal of the square of the standard error at each value of x.

Statistics

Significance tests for inference about the slope and the intercept of linear regression lines were carried out using the standard method of analysis of variance (Snedecor & Cochran, 1980). Comparison of two experimentally obtained values was made by a modified Student's t test (Snedecor & Cochran, 1980). Differences were taken as statistically significant when two-tailed probabilities less than 0.05 were obtained.

Results

Two types of non-selective cation channels activated by CCh

Figure 1 shows typical responses to superfusion of 2 μM CCh recorded in bovine ciliary myocytes by whole-cell voltage clamp at 30°C and at holding potentials (E_h) from −50 to +40 mV. CCh evoked a clear inward current at $E_h = -50$ mV. The polarity of the current was inverted at voltages higher than 0 mV (Fig. 1*A*). This response to CCh was completely abolished by 0.1 μM atropine, whereas it was not affected by verapamil or by tetrodotoxin, confirming our previous observations (Takai *et al.* 1997). In 91% of the 2678 cells examined using pipettes filled with a solution containing 180 μM GTP, the response to CCh was accompanied by a marked increase in noise (see also Fig. 2*Aa–c*). In most of these cells, discrete current steps of a constant amplitude could be readily distinguished at the onset of CCh application or

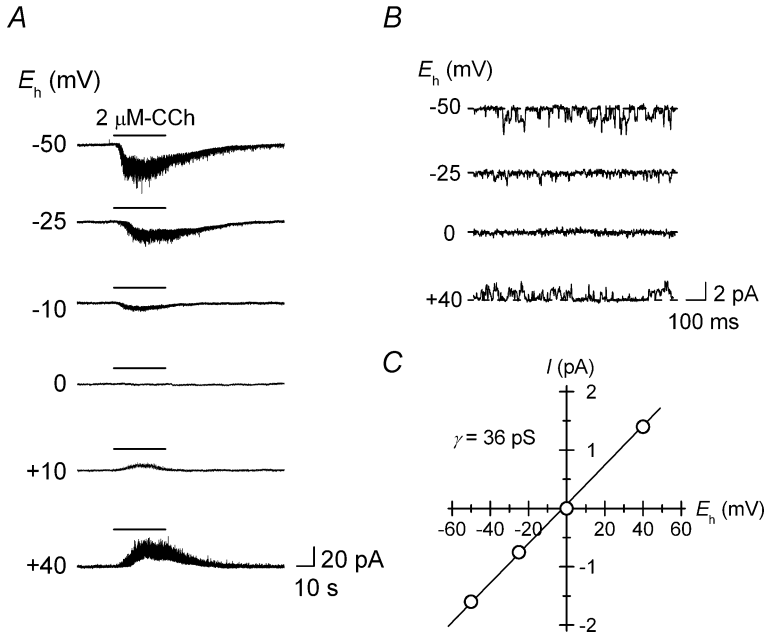

Figure 1. Whole-cell voltage–current relationship
In a smooth muscle cell freshly isolated from the bovine ciliary body, whole-cell currents were recorded at 30°C by voltage clamp using a pipette filled with a solution containing 180 μM GTP. *A*, currents elicited by application of CCh (2 μM) were recorded at six different holding potentials (E_h). CCh was applied to the bath at 5 min intervals. Note the polarity reversal at about 0 mV. *B*, single-channel currents produced by superfusion of 2 μM CCh. These recordings were taken during wash-off of the CCh so that the number of channels being activated is small. *C*, the E_h–I relationship for the current shown in *B*. The unitary slope conductance is estimated at 36 pS. See text for further explanation.

during its removal, where the number of channels being activated was small (Fig. 1*B*). The plot of the step size against E_h crossed the abscissa at a potential close to 0 mV (Fig. 1*C*), indicating that the current steps were produced by openings of a non-selective cation channel (NSCC). From the slope of the E_h–I relationship (Fig. 1*C*), the unitary conductance of the channel was estimated at 36.0 ± 0.3 pS ($n = 58$ cells). We refer to this type of NSCC with a relatively large unitary conductance as NSCCL.

When experiments were carried out at room temperature (20–23°C), the potential of polarity reversal (about 0 mV) was not changed, whereas the unitary conductance of NSCCL estimated from the discrete current steps in the whole-cell recordings was 27.3 ± 1.2 pS ($n = 17$ cells), which is significantly smaller ($P < 0.0001$) than that obtained at 30°C (see above). Thus, the unitary conductance of NSCCL exhibited a slight dependence on the temperature, with $Q_{10} = 1.2$–1.3. The effects of changing the temperature on the CCh-induced responses have not been examined further in the present experiments.

In certain cell types it has been reported that chloride channels are activated by agonists of muscarinic cholinoceptors (Dickinson *et al.* 1992) or adrenoceptors (Amédée *et al.* 1990; Wang & Large, 1991). However, in our experiments, the contribution of chloride ions to the inward currents should be little, if any, because the inward

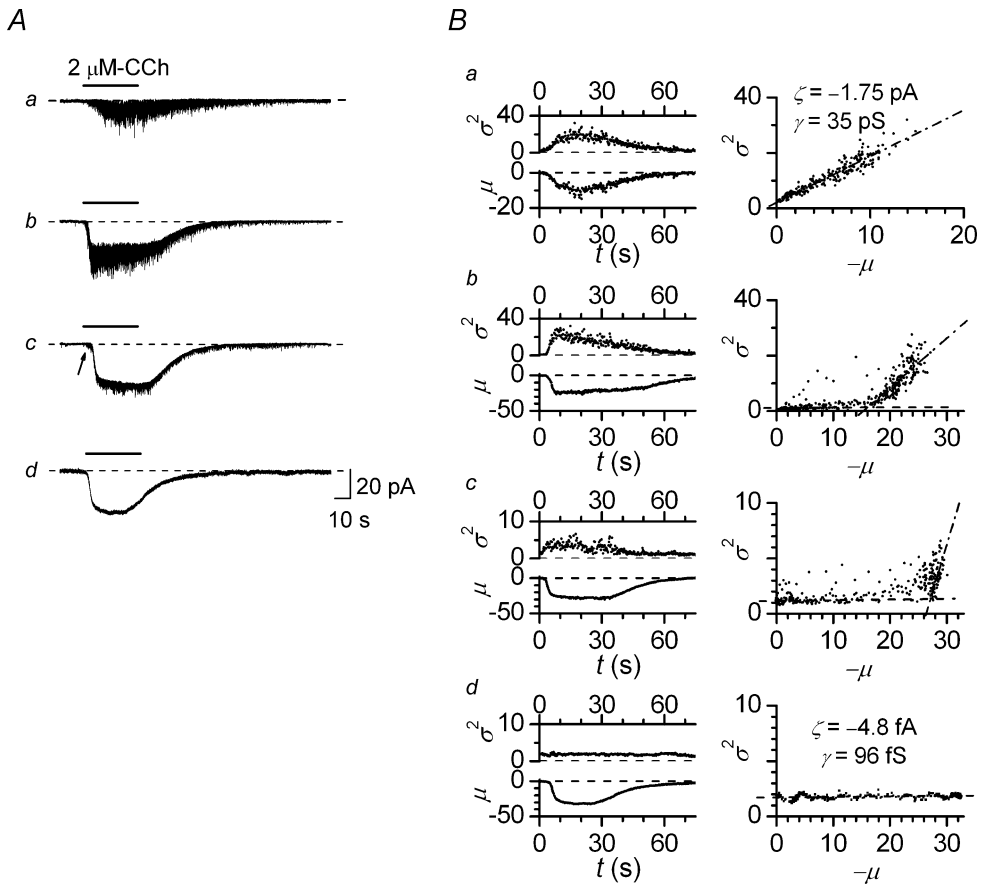

Figure 2. Inward currents evoked by CCh
Whole-cell voltage clamp recordings similar to those shown in Fig. 1. At a holding potential (E_h) of −50 mV, 2 μM CCh was applied to the bath for 30 s. *A*, whole-cell currents evoked by CCh. Four typical responses (*a*–*d*), recorded from four different cells, are shown. Note the marked difference in the noise level and mean amplitude of the currents. *B*, non-stationary variance analysis. The four records shown in *A* were low-pass filtered at 1 kHz (−3 dB, 4-pole Bessel), digitized at the sampling rate of 2 kHz, and then the mean current (μ, in pA) and variance (σ^2, in pA^2) were calculated for every 500 data points. The linear appearance of the μ–σ^2 relationships in *Ba* and *Bd* indicates that the CCh-evoked currents were produced by the opening of either NSCCL (*a*) or NSCCS (*d*) alone. The slope ζ of the regression line was −1.7 pA in *Ba* (dot–dash line) and −4.8 fA in *Bd* (dashed line), from which the unitary conductance γ was estimated, assuming the reversal potential, $E_r = 0$ mV, to be 35 pS and 96 fS, respectively. In *Bb* and *Bc*, lines of the same slopes (1.7 pA and 4.8 fA) are fitted by eye with the two apparently linear components, which are probably produced by the simultaneous opening of NSCCL and NSCCS. See text for further details.

current was clearly observed at membrane potentials around −50 mV, which is close to the equilibrium potential of chloride.

Figure 2 shows four typical patterns of the currents evoked by superfusion of 2 μM CCh under whole-cell voltage clamp at −50 mV. As noted above, the majority of the cells gave responses accompanied by a clear increase in noise (Fig. 2*Aa–c*). In these, the noise often started to appear before the change of mean current level became apparent (Fig. 2*Ac*; arrow). The intensity of noise, however, differed largely among the cells, and in many cells it did not appear to be directly correlated with the mean amplitude of the response. In the 241 other cells, CCh produced a relatively large inward current with no apparent increase in noise (Fig. 2*Ad*). In such cells, the current also changed polarity at a potential near 0 mV (see Fig. 7*B*). These observations strongly suggest that in most ciliary muscle cells CCh also opened a distinct species of NSCC with a unitary conductance much smaller than that of NSCCL, which we call NSCCS.

Figure 2*B* shows the plots of the variance σ^2 against the mean current μ for the four typical responses shown in Fig. 2*A*. In some of the cells (see Fig. 2*Ba* for example) where discrete single-channel currents attributable to openings of NSCCL were directly resolved (see Fig. 1*B*), the μ–σ^2 relationships could be well fitted with single straight lines with the slope of -1.73 ± 0.05 pA ($n = 187$ cells), from which a γ value of 34.6 pS is obtained, assuming that $E_r = 0$ mV (see eqn (2)). Since this closely agreed with the value estimated for NSCCL directly from the size of the current steps (see above), we judged that the currents of this type were almost purely produced by openings of NSCCL alone. The linearity of the μ–σ^2 relationship is indicative of a small open-state probability (see eqn (3)).

In these cells the steady-state level of the whole-cell NSCCL currents at the holding potential of −50 mV was -8.6 ± 0.4 pA ($n = 237$ responses). Since the amplitude of the single-channel current has been estimated at 1.7 pA (see above), we calculate that only five channels were open on average at any one instant during the whole-cell responses. From the whole-cell capacitance (15.7 ± 0.3 pF; $n = 187$ cells), the mean surface area of the cells was estimated at 1.6×10^3 μm^2, assuming the specific membrane capacitance of 1.0 μF cm^{-2}. The density of NSCCL open during the response to CCh is therefore calculated to be as small as 0.003 μm^{-2}. This means that approximately one NSCCL is open per 300 μm^2 of surface membrane.

Figure 2*Bd* shows another example of a μ–σ^2 relationship obtained from a cell in which CCh produced an inward current with no clear increase in noise (see Fig. 2*Ad*). Linear least-squares regression fitted the data to a straight line having a slope of -4.8 ± 0.9 fA, which is very small in magnitude compared with the values obtained for the NSCCL currents (see above) but significantly different from zero ($P < 0.001$). This indicates that the CCh-evoked response attributable to the activation of NSCCS alone was accompanied by a slight but significant increase in whole-cell current fluctuations. Similar responses to CCh with smooth appearance were observed in 241 cells, and the μ–σ^2 relationships for these responses were fitted by single straight lines of the mean slope of -4.92 ± 0.04 fA ($n = 331$ responses), from which we estimated the γ value for NSCCS at 98 fS, assuming that $E_r = 0$ mV. At the holding potential of −50 mV, the mean whole-cell currents in these cells was -25 ± 4 pA ($n = 331$ responses), which was considerably larger in absolute value than the currents produced by NSCCL alone (see above). From these results the density of NSCCS open in the ciliary myocyte membrane during a response to CCh of smooth appearance is estimated at 3 μm^{-2}. This value is 1000 times the estimate given above for the density of NSCCL channels open during a response to the same concentration of CCh.

In more than 80% of the cells examined, the μ–σ^2 relationships of the CCh-evoked whole-cell currents could not be fitted with a single straight line. In most of these responses, however, discrete single-channel currents attributable to openings of NSCCL were clearly distinguished (see Fig. 1*B*), and the μ–σ^2 relationship could be fitted with a pair of straight lines having slopes of −1.7 pA and −4.9 fA (see Fig. 2*Bb* and *c*), which probably correspond to the contributions from NSCCL and NSCCS, respectively. Generally, if an agonist simultaneously activates two types of ion channel in a cell, the μ–σ^2 plot for the whole-cell current does not necessarily resolve into two components. But if NSCCL and NSCCS are coactivated by CCh, there are several factors that combine to make the contribution from each appear as separate components in the μ–σ^2 plane. (a) The time required for the response to stimulation by 2 μM CCh to reach a steady level was 5–10 s for NSCCS currents, whereas it was 10–20 s for NSCCL currents (compare the t–μ plots of Fig. 2*Ba* and *d*); thus, NSCCS currents tended to reach a steady level (let it be μ_s) faster than NSCCL currents. This would result in a predominant appearance of the NSCCS component in the μ range between 0 and μ_s in the μ–σ^2 plane. (b) NSCCS currents showed a steady level with very small fluctuations which lasted for 15–20 s during the stimulation by CCh for 30 s (see Fig. 2*Bd*). Openings of NSCCL during this steady period would give a clearly distinguishable component in the region where $\mu \leq \mu_s (< 0)$. (c) The γ value of NSCCL (35–36 pS) was 360–380 times larger than that of NSCCS (96 fS) (see above). Reflecting this large difference in the unitary conductance levels, the contributions from NSCCL and NSCCS would appear in the μ–σ^2 plane as two linear components with largely different slopes. Thus it seems reasonable to interpret the two-component nature of the μ–σ^2 plots as a sign of the coexistence of NSCCL and

NSCCS in most bovine ciliary myocytes. The absolute value of μ_s, which can be estimated from the abscissa of the intersecting point of the two linear components, was typically 60–80% of the maximal value of $|\mu|$ ($|\mu|_{max}$; see Fig. 2*Bb* and *c*). From this percentage and the conductance ratio (360–380), the ratio of the numbers of NSCCS and NSCCL open during a typical response of the ciliary myocyte to CCh is roughly estimated at 500–2000.

Figure 3 shows the μ–σ^2 plot for a response evoked by 100 μM CCh in one of the relatively rare cells that gave a response, purely attributable to NSCCL openings alone, to a prior application of 2 μM CCh (see Fig. 2*Aa* and *Ba*). The large fluctuation of whole-cell currents due to the opening of NSCCL was also clearly observed at this agonist concentration which approaches the level required to produce the maximal response. Although the relationship between μ and σ^2 now considerably deviated from linearity (Fig. 3), it could be fitted with eqn (3) under a constraint, $\zeta = 1.75$ pA, supporting the idea that γ was not largely changed from 35 pS by the elevation of the agonist concentration. From essentially similar fits of the curved μ–σ^2 relationships for the NSCCL currents evoked by 100 μM CCh in a total of six cells, a mean total channel number N of 83 ± 8 was obtained. Significant deviation from linearity was not detected for the μ–σ^2 plots of whole-cell NSCCS currents evoked by 100 μM CCh within the limits of the resolution of the present experiments (examined in 7 cells).

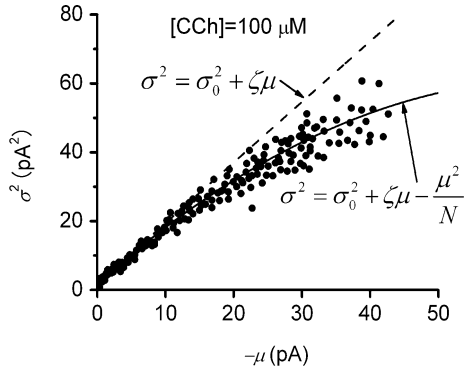

Figure 3. Non-stationary variance analysis of NSCCL current evoked by high concentration of CCh
In a cell in which 2 μM CCh invoked a response almost purely attributable to the opening of NSCCL as judged from the linear μ–σ^2 relationship (not shown), NSCCL current was evoked by a higher concentration (100 μM) of CCh. At this agonist concentration, the relationship between μ and σ^2 considerably deviated from linearity. The continuous line is a best-fit of eqn (3) obtained by non-linear least-squares regression assuming a constant single-channel current amplitude (i.e. $\zeta = 1.75$ pA). From this fit, the total number of NSCCL present in the surface membrane of this cell, N, was estimated at 77. The line, $\sigma^2 = \sigma_0{}^2 + \zeta\mu$, which is tangent to the regression curve at $\mu = 0$ pA, is also shown for comparison (dashed line). See the text for further details.

Spectral analysis

NSCCL. Figure 4*A* shows examples of the noise spectra of the whole-cell currents purely attributable to NSCCL openings evoked in the same cell under voltage clamp at −50 mV in normal PSS by different concentrations of CCh (2, 0.5 and 100 μM; applied in this order at 5 min intervals).

At 2 μM CCh, the noise spectrum obtained was well fitted with the sum of two Lorentzians (Fig. 4*A*), each being defined by the following parameters: $f_1 = 13.9$ Hz and $S_1(0) = 0.152$ pA^2 s, and $f_2 = 85.4$ Hz and $S_2(0) = 0.037$ pA^2 s (remember that $S_1(0)/S_2(0) = 4.1$). From this fit, the total variance of the CCh-evoked current was calculated in the frequency domain as $\pi f_1 S_1(0) + \pi f_2 S_2(0) = 16.6$ pA^2. Since this closely agrees with the value calculated in the time domain ($\sigma_c{}^2 = 16.8$ pA^2), it is reasonable to assume that all noise components contained in the recorded current data were represented by the two Lorentzians (see eqn (5)). Two Lorentzians were required to fit the whole-cell current noise spectra of whole-cell NSCCL currents evoked in 63 cells by 2 μM CCh, and the mean values of the corner frequencies were $f_1 = 15.3 \pm 2.3$ and $f_2 = 82.3 \pm 6.8$ ($n = 87$ spectra). The spectral function for the three-state model (Scheme 1) gave identical fits to these two-Lorentzian spectra if the following values were assigned to the rate constants: $k_1 = (1.1 \pm 0.2) \times 10^7$ s^{-1} M^{-1}, $k_2 = 109 \pm 9$ s^{-1}, $\alpha = 330 \pm 23$ s^{-1} and $\beta = 163 \pm 13$ s^{-1} ($n = 87$ spectra). These are acceptable as the rate constants for reactions involving macromolecule–ligand interactions (see, e.g. pp. 272–277 of Mahler & Cordes, 1969). In the noise spectra of the NSCCL currents evoked by 2 μM CCh in another 57 cells, only one Lorentzian with a mean corner frequency, $f_1 = 40.1 \pm 8.3$ ($n = 67$ spectra), was resolved. However, in most of these spectra the fact that two components were not detected appeared to be due to insufficient resolution at frequencies above 100 Hz.

Figure 4*Ba* summarizes the results of our experiments in which we examined the effects of changing the agonist concentration, c, on the noise spectra of the CCh-evoked NSCCL currents. As can be seen, the values of f_1, f_2 and $S_1(0)/S_2(0)$ did not change dramatically in the range $0.5\ \mu\text{M} < c < 10\ \mu\text{M}$. Consequently, the spectrum of NSCCL currents tended to be shifted upward without largely changing its shape with increasing agonist concentration in this range (compare the spectra at 0.5 and 2 μM CCh in Fig. 4*A*). Although two Lorentzians were still required to fit the five spectra for the NSCCL current evoked by 20 μM CCh, the two-component nature was obscured at this agonist concentration where the difference between f_1 (50 ± 12 Hz) and f_2 (98 ± 13 Hz) became narrower and $S_1(0)/S_2(0)$ reduced to 2.5 (spectra not shown). In the range $50\ \mu\text{M} < c < 200\ \mu\text{M}$, the spectra were well fitted with the single Lorentzian function with

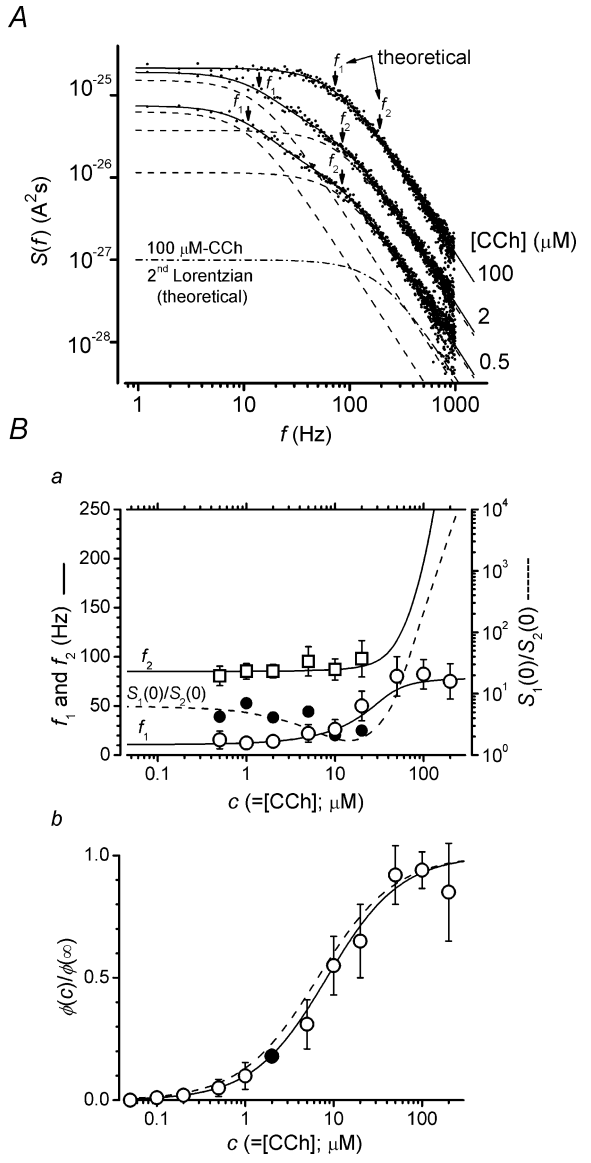

Figure 4. Power spectra of NSCCL currents
A, power spectra of the noise of the whole-cell NSCCL currents evoked in the same cell at holding potential −50 mV by three different concentrations of CCh (2, 0.5 and 100 μM, applied in this order at 5 min intervals). The records were digitized at the sampling rate of 5 Hz and digitally high-pass filtered at 0.2 Hz and low-pass filtered at 2 kHz (−3 dB, 8-pole, Butterworth). The noise data were then divided into segments each containing 4096 samples, and the spectral densities were calculated for each segment by fast Fourier transform. Seventy-two control spectral densities and 36 spectral densities during the application of CCh were averaged. The net spectra are shown, obtained by subtracting the averaged spectral densities of control noise from that during superfusion of CCh. Only the positive frequency halves of the symmetrical two-sided spectra within the frequency range 1 Hz to 1 kHz are presented. The double Lorentzian function was fitted to the data in this range by non-linear least-squares regression (continuous line). The corner frequencies (f_1 and f_2) of the Lorentzian components (dashed lines) are indicated by arrows. Note the right–upward shift of the spectrum with increasing agonist concentration. Also note the disappearance of the second Lorentzian component in 100 μM CCh. The value of the corner frequency (75.8 Hz) of this spectrum obtained by regression to the single Lorentzian function (continuous line) was only slightly larger than the value of f_1 (74.6 Hz) which was calculated together with that of f_2 (196.2 Hz), assuming the three-state kinetics. Note the low level of the second Lorentzian component calculated on the same assumption (dash–dot line). The similarly calculated first Lorentzian component (not shown) was virtually identical to the regression curve. *Ba*, effects of changing the agonist concentration on the parameters of the power spectrum. The cells used were initially stimulated by 2 μM and then by one to three other concentrations of CCh for 30 s at 5 min intervals. The values of f_1 (○), f_2 (□) and $S_1(0)/S_2(0)$ (●) for the noise spectra of NSCCL currents evoked by various concentrations of CCh are plotted against the agonist concentration, *c*. Each symbol represents the mean of at least three values. Vertical bars indicating the standard errors of the means are omitted if within symbols. The graphs of f_1, f_2 (continuous lines) and $S_1(0)/S_2(0)$ (dashed line) calculated based on the three-state model using the rate constants estimated from the spectra at 2 μM CCh are also shown. *Bb*, dose–activation relationship. The integrals of the NSCCL currents were numerically calculated. The values obtained are plotted (○) against the agonist concentration after normalization to the value for the response of each cell to 2 μM CCh (●). The continuous line is a least-squares fit of the Hill function (eqn (14)) with $\phi_{max} = 5.9$, $K = 8.4 \pm 0.5$ μM and $h = 1.1 \pm 0.1$ (total number of measurements, $n = 58$). Note that the ordinate is scaled in terms of ϕ_{max} ($= \phi(\infty)$). Dashed line is the dose–activation curve predicted from the results of the spectral analysis based on the three-state model. See text for further explanation.

corner frequencies of 75–85 Hz, and no second Lorentzian component was clearly resolved in any of the 15 spectra for the NSCCL currents evoked by CCh in this concentration range (see Fig. 4*A* and 100 μM CCh). Figure 4*Ba* includes the graphs of f_1, f_2 (continuous lines) and $S_1(0)/S_2(0)$ (dashed line) calculated based on the three-state model (Scheme 1) using the rate constants given above. These graphs appear to describe fairly well the observed changes of the spectral parameters caused by changing the agonist concentration (Fig. 4*Ba*). Based on the three-state model, the disappearance of the second Lorentzian component in the range $c > 50$ μM can mainly be attributed to the steep increase of $S_1(0)/S_2(0)$ in this range (Fig. 4*Ba*, dashed line), which corresponds to the reduction or vanishing of the A + R state caused by high concentrations of the agonist occupying R.

Figure 4*Bb* shows the dose–activation relationship for the CCh-evoked NSCCL currents which were used for the spectral analysis described above. The data were fitted with the Hill function with $K = 8.4 \pm 0.5$ μM and $h = 1.04 \pm 0.06$ (total number of measurements, $n = 58$). It is worth noting that the K value is close to the value (6.6 μM) calculated by eqn (12) using the rate constants obtained from the spectra at 2 μM (see above).

Unlike the NSCCL currents, pure NSCCS currents or the NSCCS component of CCh-evoked currents tended to become smaller when stimulation by CCh was repeated. This tendency was especially marked if the agonist concentration exceeded 10 μM. However, an essentially similar dose–activation relationship ($K = 9.3 \pm 0.7$ and $h = 1.07 \pm 0.08$; $n = 128$) was obtained in the range

0.04–10 μM CCh if responses containing a NSCCS component in various ratios ($0 < |\mu_s|/|\mu|_{max} < 0.8$ at 2 μM CCh) were included. This is consistent with the idea that CCh activates NSCCL and NSCCS through the same type of muscarinic receptor.

Using the values of the rate constants, the equilibrium probabilities of the open state of NSCCL (Scheme 1) at a given agonist concentration can also be estimated using the set of equations labelled eqn (10). At 2 μM CCh, for example, we have $p_{AR^*} = 0.08$, $p_{AR} = 0.16$ and $p_{A+R} = 0.76$. The smallness of the value of p_{AR^*} is consistent with the fact that the μ–σ^2 relationships for the NSCCL currents gave a linear appearance at this agonist concentration (Fig. 2*Ba*; see also eqn (3)).

Spectra with two Lorentzian components very similar to those obtained for the responses purely attributable to the opening of NSCCL alone were also obtained from many responses which gave μ–σ^2 plots with two components. This was not unexpected because even relatively small NSCCL currents gave spectral densities of at least an order of magnitude larger than the largest NSCCS currents over the entire frequency range where comparison could be made.

NSCCS. Spectral analysis did not resolve any clearly defined Lorentzian components in many of the cells which gave pure NSCCS currents in response to CCh (2 μM) in normal PSS at the holding potential of −50 mV. This was probably due to the limited frequency resolution as a result of the very low amplitude of the noise. Increases in noise were more clearly observed when Ba^{2+} was used as the charge carrier for NSCCS (see Fig. 7*A*). Figure 5 shows the spectrum of a NSCCS current evoked by 2 μM CCh during superfusion with a solution containing Ba^{2+} (92 mM) as the only significant cation producing an inwardly directed electrochemical gradient. It appeared evident that the spectrum had more than one Lorentzian component, even though the resolution at frequencies above 100 Hz was still limited (Fig. 5). By fitting the spectral data with the sum of two Lorentzians, we obtained the following estimates: $f_1 = 3.1$ Hz, $S_1(0) = 0.063$ pA^2 s, $f_2 = 152$ Hz and $S_2(0) = 0.00071$ pA^2 s.

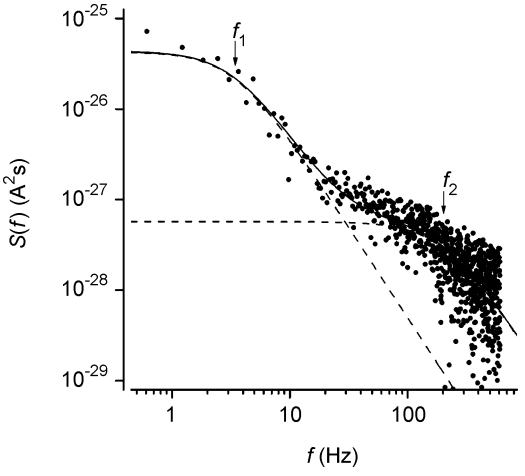

Figure 5. Power spectrum of NSCCS current
Power spectrum of the noise of the CCh-evoked NSCCS current such as the one shown in Fig. 7. CCh (2 μM) was applied during superfusion with a solution containing Ba^{2+} (92 mM) as the only significant cationic charge carrier (see the lower trace of Fig. 7*A*). This net spectrum was calculated essentially as described in Fig. 4*A*, except that the segment size was set at 8192 samples for better frequency resolution. Forty-eight control spectra and 18 spectra during the application of CCh were averaged in this case. Only the part of the symmetrical two-sided net spectra within the frequency range 0.4–600 Hz is shown. The double Lorentzian function was fitted to the data in this range by non-linear least-squares method. The corner frequencies (f_1 and f_2) of the Lorentzian components (dashed lines) are indicated by arrows. See text for further explanation.

The noise spectra of the NSCCS currents (recorded using Ba^{2+} as the charge carrier) could not be simulated by the three-state model (Scheme 1). By numerically solving eqns (6)–(9) in terms of k_1, k_2, α and β using the experimentally estimated values of μ, ζ, f_1, $S_1(0)$, f_2 and $S_2(0)$, we obtained, for the spectrum shown in Fig. 4*A*, a unique set of roots: $k_1 = -5.6 \times 10^6$ s^{-1} M^{-1}, $k_2 = 64$ s^{-1}, $\alpha = 440$ s^{-1} and $\beta = 465$ s^{-1}. The large negative value of k_1 is of course physico-chemically impossible. Non-linear least-squares regression gave no satisfactory fit if a constraint, $k_1 > 0$, was imposed. For the CCh-evoked NSCCS currents recorded in the other 21 cells using Ba^{2+} as the charge carrier, we obtained similar spectra apparently having more than one Lorentzian component with mean f_1 and f_2 values of 4.3 ± 1.2 and 159 ± 13 Hz ($n = 36$ spectra). None of these spectra could be satisfactorily simulated by the three-state model.

Relative cation selectivity of NSCCL and NSCCS

Figure 6 shows typical results of the cation-substitution experiments that we carried out in order to examine the relative cation selectivity of NSCCL. For this purpose, we chose relatively rare cells that gave a current purely attributable to NSCCL openings in response to an initial trial application of CCh (2 μM) in PSS at a holding potential of −50 mV (Fig. 6*A*, top; see also Fig. 2*Aa* and *Ba*). CCh (2 μM) was then applied to the cells at various holding potentials during superfusion with a solution containing an alkaline metal ion (Li^+, Na^+ or Cs^+; 138 mM) or an alkaline earth metal ion (Mg^{2+}, Ca^{2+}, Sr^{2+} or Ba^{2+}; 92 mM) as the only significant cationic charge carrier. From this type of experiment it was readily apparent that the alkaline metals gave a larger current than did the alkaline earths (see Fig. 6*A*). To make a quantitative comparison, we estimated the unitary current amplitude at each holding potential either by non-stationary variance analysis or by direct measurement of the size of current steps. As shown in Fig. 6*B*, the E_h–I relationships obtained differed not only in the slope but also in the reversal potential E_r,

indicating a difference in the permeability of NSCCL to the ions. Table 1 gives the values of E_r for the substitute cations (X) together with the permeability ratios P_X/P_{Na} calculated using eqn (13). We see from Table 1 that the cations fall in the permeability sequence $Cs^+ > Na^+ > Li^+ > Ba^{2+} \approx Sr^{2+} > Ca^{2+} > Mg^{2+}$. NSCCL thus exhibited a mild selectivity in favour of the monovalent cations, although it was also measurably permeable to the divalent cations including Ca^{2+}.

The effects of the total replacement of extracellular cations were also examined in the cells in which CCh (2 μM) evoked currents purely attributable to NSCCS openings. Figure 7 displays typical recordings taken from one such cell. The cell showed a current with no clear increase in noise when CCh (2 μM) was first applied in PSS at a holding potential of −50 mV (Fig. 7, upper trace). The same concentration of CCh evoked a considerably larger response accompanied by a clear increase in noise (arrow) when applied during superfusion with a solution containing Ba^{2+} (92 mM) as the only significant cationic charge carrier (Fig. 7*A*, lower trace; see Fig. 5 for the noise spectrum of a response of this type). Single-cell current amplitudes are estimated from the linear μ–σ^2 relationships (not shown) at 4 fA and 17 fA for the currents evoked in PSS and Ba^{2+}-substituted solution, respectively. To examine the voltage dependence of the current, a ramp voltage pulse falling from +120 mV to −80 mV at a constant rate of $-1\,V\,s^{-1}$ was applied before and during the application of CCh, and the voltage–current relationships were calculated as the difference between the current changes in response to the ramp pulses. As shown in Fig. 7*B*, the whole-cell current evoked in normal PSS showed inward-going rectification and changed the polarity at about −5 mV. The total cation substitution with Ba^{2+} caused a marked increase in the degree of rectification and a shift of the voltage of polarity reversal to +25 mV. Table 1 includes the permeability ratios estimated from the shifts of the reversal potential. We see now that the permeability sequence for NSCCS is $Ba^{2+} > Sr^{2+} > Ca^{2+} > Mg^{2+} > Cs^+ > Na^+ \approx Li^+$. In

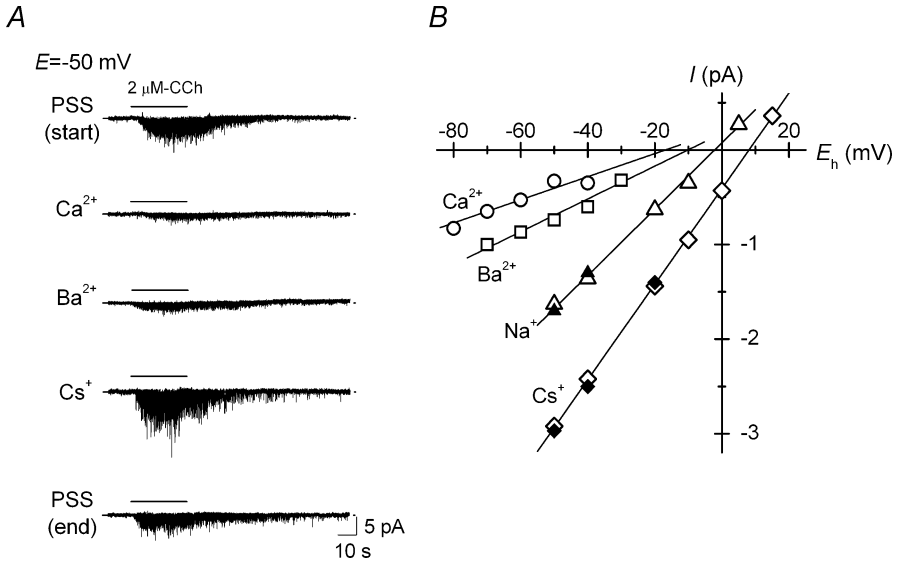

Figure 6. Effects of total substitution of the extracellular cations on NSCCL current
Na^+, K^+, Ca^{2+} or Mg^{2+} ions in the bath solution were totally replaced by alkaline metal ions (138 mM) or alkaline earth metal ions (92 mM). Whole-cell current was evoked under voltage clamp by the application of CCh (2 μM) in ciliary myocytes which gave a current mostly attributable to openings of NSCCL, as judged by non-stationary variance analysis. *A*, typical responses obtained from a cell at a holding potential (E_h) of −50 mV. The cell was first equilibrated in normal PPS and CCh (2 μM) was applied (uppermost trace). The μ–σ^2 relationship of this response was well fitted by a line with a slope of 1.7 pA (not shown). CCh was then applied to the same cell during superfusion with a solution containing only Ca^{2+}, Ba^{2+} or Cs^+ as the charge carrier. To minimize damage to the cell, the cell was rested in normal PSS for 3–5 min before each cation exchange (not shown). CCh evoked a slightly deteriorated but still clear response when applied in PSS at the end of the experiment (compare with the response at the start). *B*, the dependence of the unitary NSCCL current on E_h. In experiments similar to those shown in *A*, CCh (2 μM) was applied at various potentials during superfusion with a solution containing only Ca^{2+} (○), Ba^{2+} (□), Na^+ (△ and ▲) or Cs^+ (◇ and ◆) as the charge carrier. The unitary currents were estimated either by non-stationary variance analysis (open symbols) or by direct measurement of the size of the current steps (filled symbols) as for those shown in Fig. 1*B*. Each symbol represents the average of the values obtained from 3–4 cells. Note that the *E–I* relationships obtained using the different charge carriers differ not only in the slope but also in the reversal potential (see Table 1).

Table 1. Permeability ratios

	NSCCL			NSCCS		
Ion (X)	E_X	n	P_X/P_{Na}	E_X	n	P_X/P_{Na}
Li^+	-5 ± 2	15	0.89	-4 ± 2	7	1.0
Na^+	-2 ± 1	17	1.00	-5 ± 1	17	1.0
Cs^+	8 ± 1	18	1.45	10 ± 2	13	1.8
Mg^{2+}	-20 ± 5	15	0.28	17 ± 3	8	2.5
Ca^{2+}	-17 ± 2	24	0.33	18 ± 3	15	2.6
Sr^{2+}	-11 ± 1	16	0.45	21 ± 3	18	3.2
Ba^{2+}	-10 ± 1	21	0.47	28 ± 3	24	5.0

The permeability ratios P_X/P_{Na} for NSCCL and NSCCS were calculated from the reversal potentials (V_X; in mV) measured by the cation substitution experiments as shown in Figs 6 and 7, using eqn (13) which is based on the constant-field hypothesis. Values are given as mean ± S.E.M. n denotes the number of measurements.

contrast to NSCCL, NSCCS thus exhibited higher permeabilities to the divalent cations (including Ca^{2+} for which $P_{Ca}/P_{Na} = 2.6$) than to the monovalent cations.

On-cell patch clamp recording of the NSCCL current

Although we tried to record single-channel currents of NSCCL from on-cell membrane patches in more than 250 cells, most of the trials were unsuccessful. This was not unexpected because the density of NSCCL that were open during stimulation by CCh is extremely low, as shown above. We were only able to record CCh-evoked NSCCL openings under on-cell membrane-patch voltage clamp in six cells.

Figure 8 shows typical results obtained from one of the successful trials. The pipettes used for these experiments were filled with PSS containing 2 μM CCh and 2 μM iberiotoxin, a specific blocker of BK-type K^+ channels (Galvez *et al.* 1990), and their tips were plugged with a small amount of normal PSS containing neither CCh nor iberiotoxin by immersing in PSS and applying a weak negative pressure (−50 to −100 mmHg for 3–10 min) from the other end. The bath was perfused with high (100 mM) K^+ PSS. After establishment of giga-seal ($t = 0$ min), the potential in the pipette (E_p) was held constant at 0 mV, and a series of rectangular voltage pulses ($-E_p$ changing from −80 mV to +70 mV at 10–20 mV steps) of 250 ms duration at 5 s intervals was intermittently applied. At the start of the recording ($t = 0$–5 min; Fig. 8*A*), the opening of Ca^{2+}-dependent K^+ channels (BK type) carrying large outward current at positive potentials was often observed. Application of 2 μM CCh to the bath during this period caused no discernible change in the channel activity in the membrane patch in any of the cells examined (not shown). The BK channel stopped opening by 15 min and in the six successful trials, single-channel openings started to be observed (Fig. 8*B*). After the openings had started, they were unaffected by bath application of 10 μM atropine in any of the six trials. The plot of the unitary current amplitude against $-E_p$ (not shown) could be fitted with a straight line which crossed the $-E_p$ axis at a voltage near 0 mV, and from the slope of this regression line, the unitary conductance of 35 pS was estimated, indicating that the single-channel currents were produced by the opening of NSCCL. The BK channel activity and its gradual disappearance, the latter of which is probably due to the arrival of iberiotoxin at the extracellular surface of the membrane patch by diffusion, were observed not only in the six successful trials but also in most of the other unsuccessful trials where no NSCCL openings were observed. (Iberiotoxin (4.3 kDa) is known to inhibit BK channels at subnanomolar concentrations (Galvez *et al.* 1990), whereas at least 0.1 μM CCh (147.19 Da) is required to activate NSCCL (see Fig. 4*Bb*). Given such an exceedingly high affinity of iberiotoxin to BK channels, it is not surprising that the effect of iberiotoxin, which has a larger molecular size than CCh, usually appeared earlier than did that of CCh. Despite the relatively large difference in the molecular sizes, the ratio of the diffusion coefficients of CCh and iberiotoxin is estimated to be at most 5, using the well-known rule of thumb that the diffusion coefficient is inversely proportional to the cube root of the molecular mass.) In two of the six cells, the number of open channels gradually increased and reached a steady level by 20–30 min (Fig. 8*C*), but in the other four cells such an increase did not occur and only a small number of NSCCL openings continued to be observed for more than 60 min (not shown). The reason for this difference is not clear from the present experiments.

These observations support the idea that the components of the signalling pathway for NSCCL activation is confined within a narrow area of the membrane, so that the signal cannot spread beyond the seal of the patch pipette (see Discussion).

Possible involvement of G-protein-dependent pathway in the muscarinic signal transduction

When we used pipette solutions containing no GTP, as we did in our previous experiments (Takai *et al.* 1997), currents accompanied by a clear increase in noise were observed in only 38 out of the 254 cells which gave clear inward currents in response to 2 μM CCh at the holding potential of −50 mV. In contrast, the presence or absence of GTP in pipettes did not change the properties of the NSCCS currents to a considerable degree. For CCh-evoked currents of smooth appearance recorded from 218 cells using a pipette solution containing no GTP, variance analysis estimated a mean ζ value of 4.88 ± 0.06 fA ($n = 288$ responses), which is not significantly different from the value given above for the NSCCS currents recorded using a pipette solution containing GTP.

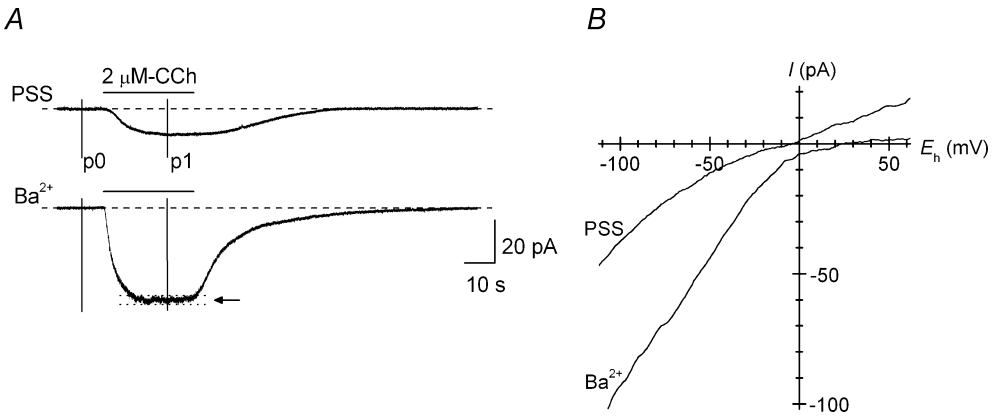

Figure 7. Effects of substitution of the charge carrier on the NSCCS current
A, whole-cell currents evoked by bath application of 2 μM CCh at a holding potential of −50 mV in a ciliary myocyte which showed a current purely attributable to NSCCS openings (cf. Fig. 2*A*d) in response to the application of CCh (upper trace). The same concentration of CCh evoked a larger response accompanied by a slight but clear increase in noise (arrow) when Na^+, K^+, Ca^{2+} and Mg^{2+} were isosmotically replaced by 92 mM Ba^{2+} (lower trace; see Fig. 5 for a power spectrum for this type of response). Unitary current amplitudes of 4 fA and 16 fA are estimated from the linear μ–σ^2 relationships (not shown) for the currents in PSS and Ba^{2+}-substituted solution, respectively. To examine the voltage dependence of the current, a ramp voltage pulse falling from +120 to −80 mV at a constant rate of -1 V s^{-1} was applied before (p0) and during (p1) the applications of CCh. *B*, the voltage–current (E_h–*I*) relationships calculated as the difference between the responses to the ramp pulses (p1 minus p0). The current evoked in PSS showed inward-going rectification and changed the polarity at about −5 mV. The total cation substitution with Ba^{2+} caused a marked increase in the degree of rectification and a shift of the voltage of polarity reversal to about +25 mV.

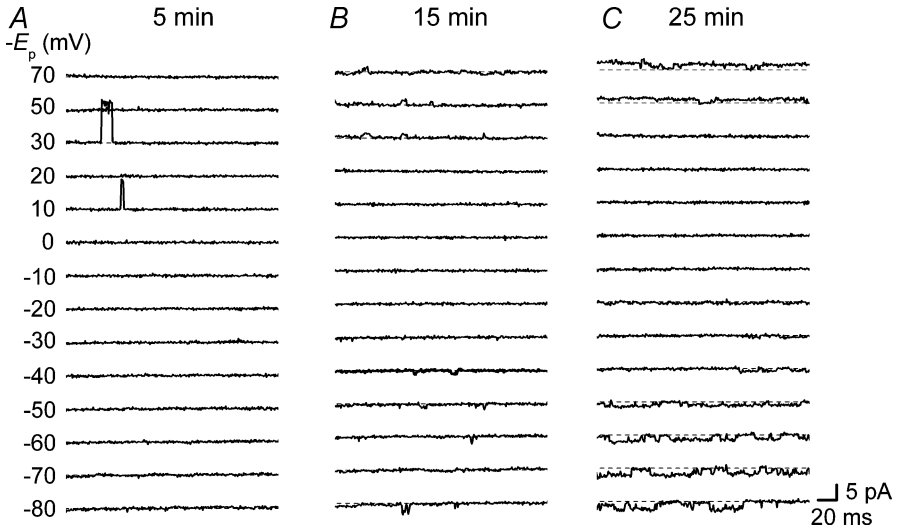

Figure 8. Unitary NSCCL openings recorded under on-cell membrane-patch voltage clamp
Voltage clamp recordings from an on-cell membrane patch. The pipette used was filled with PSS containing 2 μM CCh and 2 μM iberiotoxin, and its tip was plugged with a small amount of normal PSS containing neither CCh nor iberiotoxin by immersing in PSS and giving suction from the other end. The bath was perfused with high K^+ (100 mM) PSS. After establishment of a giga-seal ($t = 0$ min), the potential in the pipette (E_p) was held constant at 0 mV, and a series of rectangular voltage pulses ($-E_p$ changing from −80 mV to +70 mV in 10–20 mV steps) of 250 ms duration at 5 s intervals was intermittently applied. The responses elicited by the voltage pulse series at 5 min (*A*), 15 min (*B*) and 25 min (*C*) are shown. In the early stage (0–10 min), opening of a Ca^{2+}-dependent K^+ channel (BK type) carrying large outward current at positive potentials was often observed (*A*). As the BK channel stopped opening by 15 min, probably due to the arrival of iberiotoxin at the extracellular surface of the membrane patch by diffusion, single-channel openings of NSCCL began to be observed (*B*). In this and one other cell, the NSCCL openings gradually increased and reached a steady level by 20–25 min (*C*). In the other 4 cells where single-channel openings of NSCCL were observed, such an increase did not occur and only an small number of openings continued to be seen for more than 60 min (not shown). See text for further details.

As shown in Fig. 9*A*, replacement of GTP in the pipette solution with its poorly hydrolysable analogue GTPγS gradually caused spontaneous opening of NSCCL in the absence of CCh, suggesting a G-protein-linked signalling mechanism. CCh (2 μM), when applied 1–2 min after the establishment of the whole-cell configuration, accelerated the appearance of the effect of GTPγS (Fig. 9*B*). In 9 out of the 11 cells in which similar results were obtained, CCh not only activated NSCCL but also caused a marked change in the mean current level, which was probably caused by opening of NSCCS (Fig. 9*B*). The effect on the mean current level was reversible, in contrast to that on NSCCL which was sustained after removal of CCh. Essentially the same results were obtained if the concentration of GTPγS was increased to 360 μM (observation in 2 cells). These results suggest that the signals from the muscarinic receptors are sent to NSCCL by a G-protein-linked mechanism whereas they reach NSCCS through some different pathway which might conceivably be independent of G-proteins (see Discussion).

The responses to CCh (2 μM) were not affected when either pertussis toxin (0.1 μg ml^{-1}; examined in 23 cells) or cholera toxin (1 μg ml^{-1}; examined in 11 cells) was added together with 100 μM dithioerythritol to the pipette solution containing GTP (180 μM).

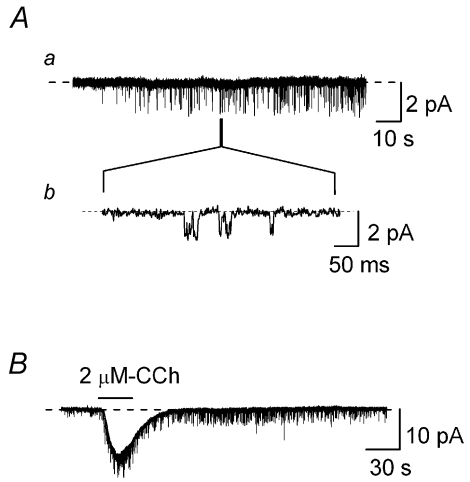

Figure 9. Activation of NSCCL by intracellular application of GTPγS
Whole-cell currents were recorded using pipettes filled with solution containing 180 μM GTPγS in place of GTP. The membrane potential was clamped at −50 mV. *Aa*, 5–10 min after establishment of the whole-cell configuration, spontaneous openings of NSCCL were observed in the absence of CCh. *Ab*, part of the trace is presented on an expanded time scale, to show unitary channel openings. *B*, application of CCh (2 μM) accelerated the appearance of the effect of GTPγS. CCh not only activated NSCCL but also caused a marked change in the mean current level indicating activation of NSCCS. Note that the effect on the mean current level was reversed, whereas that on NSCCL was sustained, after removal of CCh.

Inhibitory effect of intracellular Ca^{2+} on NSCCS

Figure 10 shows the effects of increasing the intracellular Ca^{2+} concentration $[Ca^{2+}]_i$ on the CCh-induced currents. The bath was perfused with normal PSS or a solution in which alkaline and alkaline earth cations in PSS were totally replaced with either Ba^{2+} or Sr^{2+}. The pipettes used were filled with solution containing 70 or 400 nM free Ca^{2+}. It has been shown in several mammalian cells that elevation of $[Ca^{2+}]_i$ activates some types of non-selective cation channel. In the bovine ciliary muscle, however, the current elicited by CCh was suppressed by nearly 80–85% when $[Ca^{2+}]_i$ was increased from 70 to 400 nM (Fig. 10; PSS), confirming our previous observations (Takai *et al.* 1997). Still more marked (90–95%) reduction of the current amplitude was observed when the extracellular cations were totally replaced with Ba^{2+} or Sr^{2+}, to which NSCCS exhibits considerably higher permeabilities than it does to monovalent cations (see Table 1 above). In our previous experiments, the opening of NSCCL was clearly observed even when the $[Ca^{2+}]_i$ was increased to 700 nM, indicating that NSCCL is much less sensitive to elevation of $[Ca^{2+}]_i$. The reduction of the CCh-induced current caused by increasing $[Ca^{2+}]_i$ thus appears to be due mostly to inhibition of NSCCS.

Inhibition of NSCC currents and isometric tension by SKF96365, Ga^{2+} and La^{3+}

As shown in Fig. 11*A*, the CCh-induced currents in the bovine ciliary muscle were inhibited in a dose-dependent manner by SKF96365, a compound generally used as a blocker of receptor-operated NSCCs (Merritt *et al.* 1990).

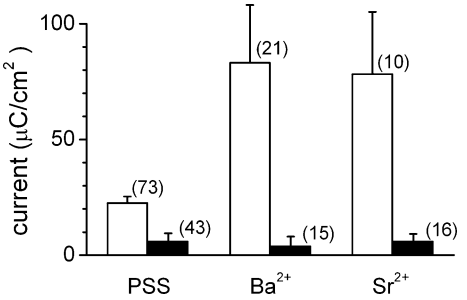

Figure 10. Inhibitory effect of intracellular Ca^{2+} on NSCCS
The integrals of the inward currents invoked by bath application of 2 μM CCh for 30 s were compared. The bath was perfused with either normal PSS or a solution in which alkaline and alkaline earth cations in PSS were isosmotically replaced with either Ba^{2+} or Sr^{2+} to which NSCCS exhibits relatively high permeabilities (see Table 1). Pipettes used were filled with solution containing 70 nM (open columns) or 400 nM free Ca^{2+} (filled columns). The values are normalized to the area of the cell membrane estimated from the whole-cell capacitance. The numbers in parentheses are the number of cells examined and the vertical lines indicate the standard errors of the means. The marked reduction of the Ba^{2+} and Sr^{2+} currents by increasing the intracellular Ca^{2+} concentration is indicative of a strong inhibitory effect of intracellular Ca^{2+} on NSCCS.

After fitting eqn (14) to the dose–inhibition data the values of K and h were estimated to be $0.76 \pm 0.15\ \mu$M and 0.8 ± 0.1, respectively (number of measurements, $n = 33$). As shown in Fig. 11*B*, the currents were also dose-dependently inhibited by La^{3+} ($K = 12 \pm 4\ \mu$M and $h = -1$ (fixed); $n = 37$) and Gd^{3+} ($K = 7 \pm 1\ \mu$M and $h = -1$ (fixed); $n = 37$), two of the other putative NSCC blockers (Docherty, 1988; Popp *et al.* 1993). The mean amplitude of the currents approached a zero level in the presence of higher concentrations ($> 100\ \mu$M) of these blockers, indicating that both NSCCL and NSCCS are sensitive to them.

As shown in Fig. 12*A*, the contractile response produced by 2 μM CCh had an initial phasic component which was followed by a tonic component. Removal of Ca^{2+} from the bath solution had relatively little effect on the phasic component, whereas it abolished the tonic component, which was quickly restored by readmission of 2.4 mM Ca^{2+}.

Figure 12*B* shows the effect of SKF96365 (100 μM) on the contraction evoked by the same concentration (2 μM) of CCh. As can been seen, the tonic component was strongly inhibited by SKF96365, whereas the initial phasic component clearly remained even in the presence of this substance. Figure 12*C* shows the dose–inhibition relationship for the effect of SKF96365, which was well fitted by eqn (14) with $K = 1.3 \pm 0.3\ \mu$M and $h = -0.9 \pm 0.1$ ($n = 21$). The contraction produced by CCh (2 μM) was also inhibited by La^{3+} ($K = 9 \pm 4\ \mu$M and $h = -1$ (fixed); $n = 13$) and Gd^{3+} ($K = 5 \pm 4\ \mu$M and $h = -1$ (fixed); $n = 15$) (dose–inhibition curves not shown). Thus, SKF96365, La^{3+} and Gd^{3+} inhibited the CCh-evoked NSCC currents and contractions in nearly the same concentration ranges.

Figure 12*D* shows the relationship between the agonist concentration (0.1–316 μM CCh) and the amplitude of the tonic tension. The dose–activation relationship was well fitted with the Hill function with $K = 5.4 \pm 1.5\ \mu$M and $h = 1.08 \pm 0.05$ (total number of measurements, $n = 27$). These are in close agreement with the values ($K = 6.9\ \mu$M and $h = 1.0$) previously reported for CCh-induced isometric tension developments in the rabbit ciliary muscle (Konno & Takayanagi, 1985). It is noteworthy that the contractile response (Fig. 12*D*) and the whole-cell current response (see Fig. 4*Bb*) induced by CCh exhibited very similar dose dependence (see Discussion).

Search for TRPC mRNAs by RT-PCR

We examined the existence of transcripts of the *trpc*1–7 genes (which encode TRPC1-7 channel proteins) in the bovine ciliary muscle (whole tissue) by RT-PCR. Figure 13 shows a typical agarose gel image taken after electrophoresis of the PCR products, and Table 2 summarizes the results obtained by the PCR experiments.

The PCR using the primer pairs for TRPC1, TRPC3, TRPC4 and TRPC6 yielded amplified cDNA fragments of the expected sizes (Fig. 13). (Table 3 compares several characteristic properties of NSCCL and NSCCS with those reported for these TRPs in the literature.) It was confirmed that the amplified cDNA fragments were identical to the corresponding TRPC cDNA of the other bovine tissues in the nucleotide sequence of the regions for which reference data were available from the GenBank database (Table 2). No reference data from bovine tissues were available in the GenBank for a middle 396 bp segment of the 1071 bp TRPC3 cDNA fragment as well as for the entire region of the 286 bp TRPC6 cDNA fragment whose sense-strand has an ATG initiation codon at the 15–17th position from the 5′ end. The nucleotide sequences of these fragments

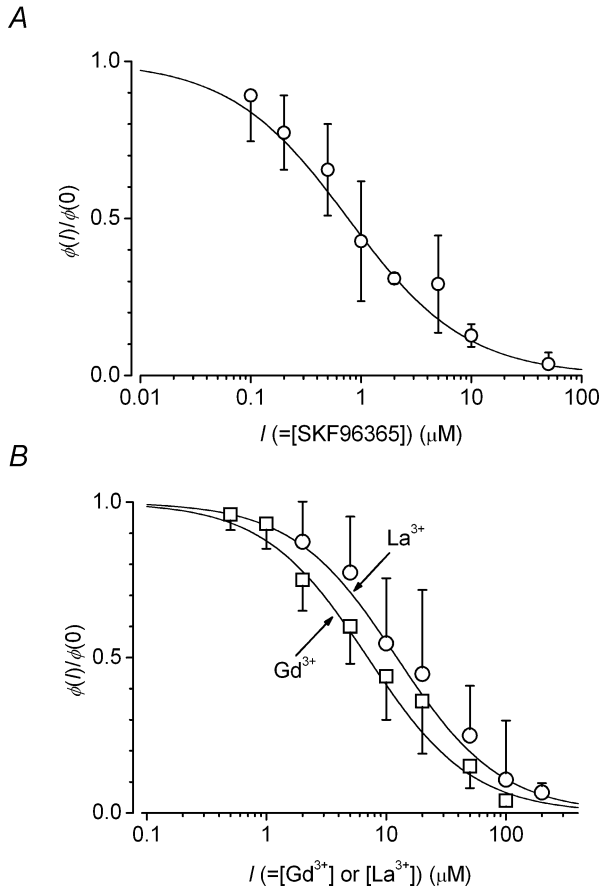

Figure 11. Inhibitory effect of Ga^{3+}, La^{3+} and SKF96365 on the NSCC currents

Under whole-cell voltage clamp at −50 mV, 2 μM CCh was superfused for 30 s in the presence of various concentrations (I) of SKF96365 (*A*), Ga^{3+} and La^{3+} (*B*) in the bath solution. Ga^{3+} and La^{3+} were applied in the presence of 0.5 mM ascorbic acid as the antioxidant, which was also added when $I = 0\ \mu$M. The integral of the currents invoked by CCh were calculated and normalized to the values in the absence of the inhibitors ($= \phi(0)$). The curves are least-squares fits of the Hill function (eqn (14)). Each symbol represents the average of at least 3 values obtained from 3–5 cells. The vertical lines indicate the standard errors of the means.

(AB179743 and AB180232) were 88–99% identical to the corresponding regions of the cDNA sequences of the TRPC homologues of the other mammalian species (Table 2). Notably, the difference between the present and the reference sequence data almost always occurred in the third nucleotide of the codon, and the identity was not less than 98.5% in any of the cases if comparison was made between the amino acid sequences deduced from the nucleotide sequences. The primer pairs for TRPC2, TRPC5 and TRPC7 (Table 2) did not yield amplification products under the present PCR conditions.

The existence of transcripts of the *trpv* and *trpm* genes (see Clapham *et al.* 2001; Minke & Cook, 2002; Inoue *et al.* 2003) in the bovine ciliary muscle has not been examined in the present experiments.

Discussion

The present whole-cell voltage clamp experiments, most of which were carried out at 30°C using pipettes filled with solution containing GTP (180 μM), have revealed that stimulation of atropine-sensitive cholinoceptors by CCh simultaneously invokes two types of NSCC openings with widely different unitary conductance levels (35 pS and 100 fS) in the great majority of the bovine ciliary smooth muscle cells. The plot of the variance against mean current (μ–σ^2 plot) has often clearly resolved two components corresponding to the 35 pS and 100 fS openings (see Fig. 2). The relative intensity of the noise attributable to each of these openings largely varies among the cells. Since there appears to be no obvious interdependence between

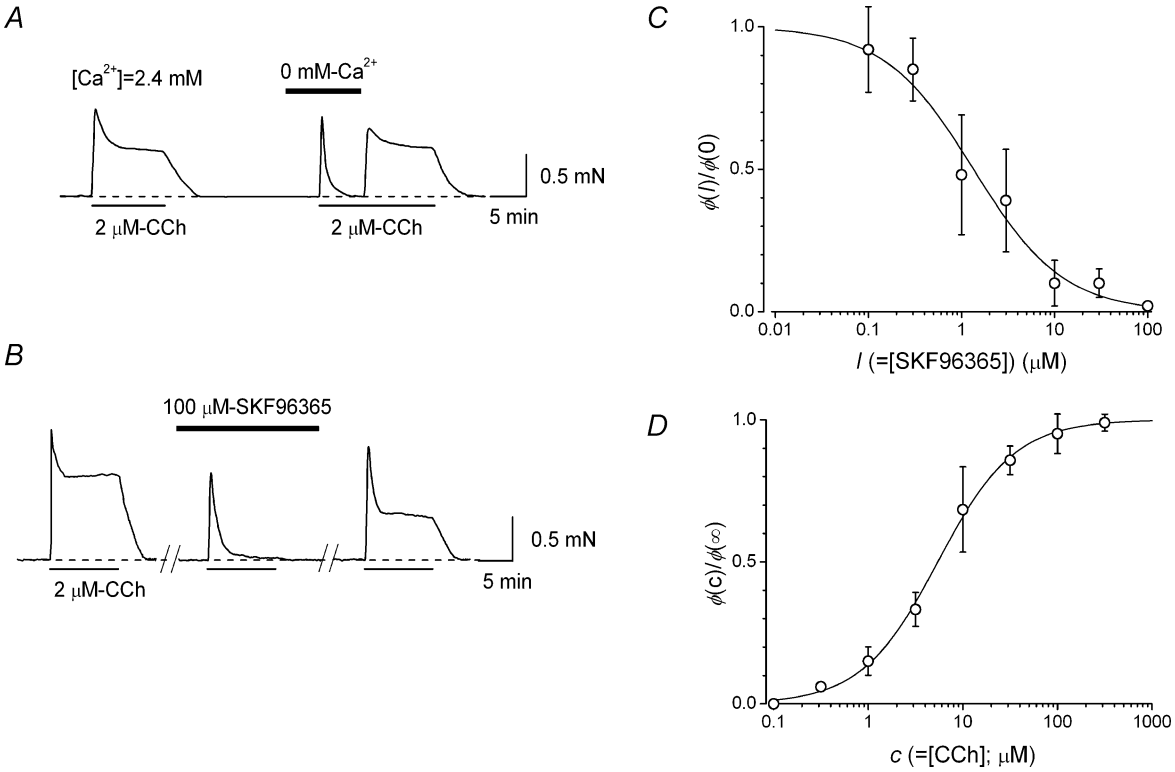

Figure 12. Effects of Ca^{2+} removal and SKF96365 on the isometric tension development produced by CCh

Isometric tension development in response to bath application of CCh (2 μM) was recorded in the ciliary smooth muscle bundles. *A*, CCh (2 μM) produced a sustained contraction in normal PSS (*A* and *B*) whereas it produced only a transient phasic contraction when it was applied in Ca^{2+}-free PSS containing 0.2 mM EGTA. *B*, 100 μM SKF96365 inhibited the tonic component without strongly affecting the phasic component of the CCh-induced contraction. The inhibition of the tonic component of the contraction by SKF96365 was clearly but only partially recovered when SKF96365 was washed out for 30 min. *A* and *B* were records from different preparations. *C*, the relationship between the concentration of SKF96365 and the tonic tension. The levels of the tonic component of the contraction induced by 2 μM CCh are plotted against the concentration of SKF96365. *D*, the relationship between the agonist concentration and the mechanical response. The levels of the tonic component of the CCh-induced contraction are plotted against the agonist concentrations (0.1–316 μM). In *C* and *D*, the values have been normalized to $\phi(0)$ and $\phi(\infty)$, respectively, and each point represents the mean of 3 values. Vertical bars indicating the standard errors of the means are omitted if within symbols. The curves are least-squares fits of the Hill function (eqn (14)). See the text for further details.

the two types of opening, we assume here as in the rest of the paper that the two conductance levels correspond to openings of two different types of NSCC (NSCCL and NSCCS) rather than to substates of a single species of NSCC.

In addition to the wide difference in the unitary conductances, we have identified several characteristics which clearly distinguish NSCCL and NSCCS from each other. We will first consider such characteristic differences and then discuss implications for the functional roles for these NSCC types in the ciliary muscle contraction. We will also discuss the possible relationship of the NSCCs to the TRPC channels whose mRNAs have been detected in the present RT-PCR experiments.

Differences between NSCCL and NSCCS

Single-channel conductances. It is known that NSCCs activated in various smooth muscles by agonists including acetylcholine (Inoue *et al.* 1987; Janssen & Sims, 1992) and noradrenaline (Wang *et al.* 1993; Inoue & Kuriyama, 1993) display similar single-channel conductances typically ranging from 20 to 30 pS under near-physiological ionic conditions. The value for NSCCL (35 pS) slightly exceeds the upper boundary of this range. However, it should be noted that most of the conductance values found in the literature are based on experiments at room temperature (20–26°C) and that the unitary conductances of ion channels are generally somewhat temperature dependent (see, e.g. Hoffmann & Dionne, 1983). The value for NSCCL (27 pS) obtained at room temperature (20–23°C) in the present experiments is within the above-mentioned range.

The present noise analysis has estimated the unitary conductance of NSCCS at 100 fS, which is 350–360 times smaller than that of NSCCL (measured at 30°C). To the best of our knowledge, this is the first demonstration that muscarinic stimulation activates a NSCC with a unitary conductance in the femtosiemens range in smooth muscle cells. Unitary conductances in the range 2–5 pS have been reported for store-operated NSCCs of vascular myocytes (Trepakova *et al.* 2000, 2001; Golovina *et al.* 2001; Albert & Large, 2002) and an ATP-activated NSCC of rat vas deferens myocytes (Friel, 1988). The unitary conductance of NSCCS observed in the present experiments is still one order of magnitude smaller. In some preparations of rat cerebellar granule cells, it has been shown by noise analysis that glutamate and kainate activate a channel with a unitary conductance of approximately 140 fS which is comparable with the value for NSCCS (Cull-Candy *et al.* 1988). The very small unitary conductance of NSCCS, which admits Ca^{2+}, may be useful for a smoothly graded adjustment of $[Ca^{2+}]_i$ in ciliary muscle cells (see below).

Number of channels. Because of its relatively large unitary conductance, openings of NSCCL can directly be detected as discrete current steps under voltage clamp

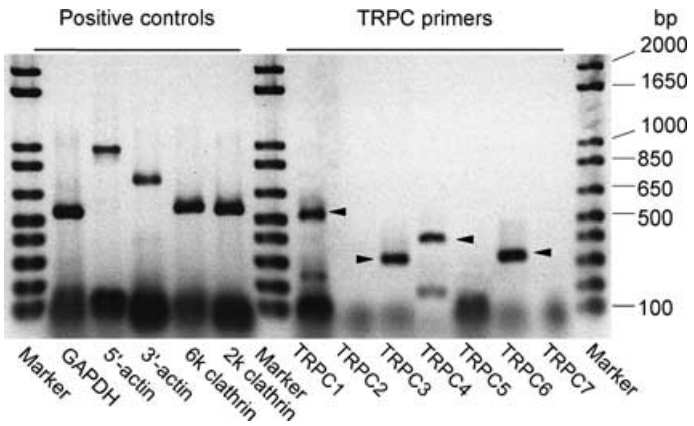

Figure 13. Detection of TRPC transcripts in bovine ciliary muscle by RT-PCR
The existence of TRPC mRNAs in the bovine ciliary muscle (whole tissue) was examined by RT-PCR. A typical agarose-gel image taken after electrophoresis of the PCR products is shown (brightness inverted). Each PCR reaction mixture contained 10^{-18} M cDNA as the template. The PCR reactions with the five positive-control primer pairs and four bovine TRPC-specific primer pairs yielded DNA fragments of the expected sizes (in parentheses; unit, bp): GAPDH (540), 5′actin (1000), 3′actin (720), 6 kb clathrin (570), 2 kb clathrin (550), TRPC1 (259), TRPC3 (323), TRPC4 (382) and TRPC6 (321). The bands of the amplified TRPC DNA fragments are indicated by arrowheads. The results of the sequence analysis using the DNA fragments extracted from the bands have been deposited in the GenBank under the accession numbers which are given in Table 2 together with the sequences of the primer pairs used. The TRPC3-specific primers (not listed in Table 2) used in this PCR experiment were 5′-CCAGCAGCAGCTCTTGAC-3′ (forward) and 5′-ACTGTGTGGTTTTCACCCTG-3′ (reverse), which amplify an initial 323 bp segment of the 1071 bp fragment (AB179743) listed in Table 2. The primers for TRPC2 (expected size in bp, 206), TRPC5 (275) and TRPC7 (830) gave no specific amplifications.

Table 2. Search for TRPC mRNAs in bovine ciliary muscle by RT-PCR

Present RT-PCR experiments (bovine ciliary muscle)					Reference sequences		
Type	Primer pairs (Forward/Reverse; 5′→3′)	Expected size (bp)	Accession number	Identity (%)	Accession number	cds (full or partial)	Sources
TRPC1	GACAGATGTCAGGTTACC ATTCTTTCAAGGGCTGGC	259	AB179741	100	AF012900	Full	Bovine aortic endothelial cells
	TACTGTGGATTATTGGAATGA CAGAACAAAGCAAAGCAAGTG	505	AB179742	100	AF012900		
TRPC2	ATGGTCATCCTCTCCCTGTACC TCAGGTCCCCTCCTTGGCTCC	1299	n.d.	—	AJ006304	Full	Bovine testis
	CACTTCTGCTGCAAAACC AGCTCTGTCAGTCTGTTG	206	n.d.	—			
TRPC3	CCAGCAGCAGCTCTTGAC ACTGTGTGGTTTTCACCCTG	1071	AB179743*	100	AJ006781	Partial	Bovine arterial endothelial cells
				100	AF012902	Partial	
				92	U47050	Full	Human (HEK 293 cells)
				94	AB090949**	Full	Guinea-pig ileum
TRPC4	CTGCTGGCGTCTCGCTGGTAC AGGACCCACGGTAATATC	306	AB179744	100	X99792	Full	Bovine retina and adrenal gland
	CTGCAGATATCTCTGGGAAGA CCGCATGGTCAGCAATAAG	382	AB179745	100	X99792		
TRPC5	GTACTGCTGGCTTTTGCC TTCAGCAGCACTACCAGG	275	n.d.	—	AJ271070	Partial	Bovine brain
TRPC6	GACATCTTCAAGTTCATGGTCATA ATCAGCGTCATCCTCAATTTC	321	AB179746	100	AJ271069	Partial	Bovine adrenocortical cells
				96	AF080394	Full	Human testis and placenta
				90	U49069	Full	Murine brain
				94	AB090950**	Full	Guinea-pig ileum
	GAGGACCAGCATACAT ACAATCCGAACATAAC	286	AB180232*	92	AF080394	Full	Human testis and placenta
				88	U49069	Full	Murine brain
				99	AB090950**	Full	Guinea-pig ileum
TRPC7	TACTTCTGCAAGTGCAATGAGTGC TTCCACAAGTGTAGCACGTACTCCC	830	n.d.	—	AF139923	Full	Murine brain
					NM003307	Full	Human brain
	CGGCACACCACCTTGAGGGAG CCCAAACTTCTCGCTGAGCTGCTGA	2502	n.d.	—			
	CGCTTCTCCCACGACATCACACCC GTGGAAGTGAGACGTTGTGCAG	1078	n.d.	—			

The existence of transcripts of *trpc*1–7 genes (which encode TRPC1–7 proteins) in the bovine ciliary muscle (whole tissue) was tested by RT-PCR, using the gene-specific primer pairs listed. The PCR reactions with the primer pairs for TRPC1, TRPC3, TRPC4 and TRPC6 yielded DNA fragments of expected sizes (see Fig. 13). The sequence data for the DNA fragments have been deposited in the GenBank under the accession numbers given in the list. The primer pairs for TRPC2, TRPC5 and TRPC7 gave no specific amplifications. The reference sequences (obtained from the GenBank) used for the design of the PCR primers and for the identification of the amplified DNA fragments are also listed. The percentages of the identity of nucleotide sequences between the present data and the corresponding segments of the reference sequences were calculated. Abbreviations and symbols: n.d., no specific amplification detected; cds, coding DNA sequence ('full' and 'partial' indicate whether each reference sequence contains a full cds or only a partial cds); * cDNA sequence data including a region for which no GenBank data had been available for any bovine tissue before the present work; ** our unpublished sequence data.

in whole-cell (Fig. 1*B*) and on-cell membrane-patch recording configurations (Fig. 8). The single-channel currents of NSCCS, in contrast, are too small to resolve with our present recording system. It appears, however, that openings of NSCCS far outnumber those of NSCCL in the majority of the cells. The present non-stationary variance analysis has made an estimate as small as 80 per cell for the total number of NSCCL in cells in which CCh

Table 3. Comparison of NSCCL and NSCCS with TRPC channels

Channel	γ (pS)	P_{Ca}/P_{Na}	Effect of $[Ca^{2+}]_i$	References
NSCCL	36, 35† (30°C) 27 (20–22°C)	0.33	Little or no effect	Present work
NSCCS	0.1† (30°C)	2.6	Suppression	Present work
TRPC1	16†	1.3–2.1‡	?	Zitt *et al.* (1996)
TRPC3	23†, 66	1.5	Activation	Zitt *et al.* (1997), Kamouchi *et al.* (1999)
TRPC4	41	1, 8, 160	?	Philip *et al.* (1996), Schaefer *et al.* (2000), Freichel *et al.* (2001)
TRPC6	35, 28	5	Activation	Hofmann *et al.* (1999), Inoue *et al.* (2001)

Some channel properties of NSCCL and NSCCS are compared with those of the TRP homologues whose mRNAs were detected in the present RT-PCR experiments. Note that the data for the TRPC homologues from the references are all based on electrophysiological experiments at room temperature (20–26°C). Symbols: † γ value estimated by noise analysis; ‡ permeability ratio calculated by eqn (13) using the data of the cation substitution experiments described in the reference.

evoked currents purely attributable to opening of this type of channel (Fig. 3). The number of NSCCL open at any instant during stimulation with 2 μM CCh is calculated, from the mean whole-cell currents and the unitary current amplitude, to be at most only 10 per cell even in the ciliary myocytes which give very large current noise. From the relative position and extent of the two linear components in the μ–σ^2 plots, it is estimated that the number of NSCCS open is 500–2000 times that of NSCCL and more than half (60–80%) of the current flows through NSCCS during a typical response of the ciliary muscle cell to CCh (see Results).

Kinetics. The present spectral analysis of the NSCCL currents produced by relatively low concentrations (0.5–10 μM) of CCh has resolved two Lorentzian components in most cases (Fig. 4*A*). One of the most important limitations to our present kinetic analysis has been that we could not check more directly the adequacy of the rate constants estimated from the spectral data in single-channel levels, mainly because of the very sparse distribution of NSCCL. However, at least we have shown that the three-state model simulates the two-component nature of the spectra well and provides reasonable explanations for the effects of changing the agonist concentration on the kinetics of the NSCCL currents. (a) The large fluctuation of whole-cell currents due to the opening of NSCCL tends to increase as the concentration of CCh is increased, and it has also been very clearly observed at 100 μM CCh which approaches the level required to produce the maximal response (see Fig. 3). Thus, CCh cannot open all NSCCL even at high concentrations. This phenomenon, which is contrary to the predictions of the classical two-state model $A + R \leftrightarrow AR^*$, can readily be explained by the three-state model (see Colquhoun & Hawkes, 1977). (b) We have shown that the two-component nature of the spectra of NSCCL currents becomes obscured as the agonist concentration exceeds the apparent dissociation constant K and one of the two Lorentzians completely disappears at higher agonist concentrations (see Fig. 4*A*). According to the three-state model, the reduction of the number of Lorentzian components from two to one can most simply be understood as a consequence of the reduction or vanishing of one of the three states, A + R, due to binding of R with high concentrations of the agonist (see Fig. 4*Ba*). (c) We have shown that the relationship between the agonist concentration and the amount of CCh-evoked NSCCL current is well described by the Hill function with $K = 8.4$ μM and $h = 1.04$. These values of K and h closely agree with the values ($K = 6.6$ μM and $h = 1$) predicted by the calculations based on the three-state kinetics (see Fig. 4*Bb*).

Although the noise spectra for the NSCCS currents also appear to have two Lorentzian components, we have shown that there exists no physico-chemically reasonable set of values of rate constants which gives a satisfactory fit of the spectral function derived for the three-state model to the spectra. Given the limited resolution of the present spectral analysis, we cannot exclude the possibility that the noise spectra of NSCCS actually have some small Lorentzian components which have escaped detection. If there are such additional Lorentzians, we will need to adopt a more complex model with four or more states to simulate the kinetic properties of NSCCS.

Cation permeability ratios. The two types of NSCC are also clearly different in their relative permeabilities to alkali and alkaline earth metal ions as well. We have shown that NSCCL exhibits a mild ion selectivity in favour of the monovalent cations (see Table 1). The relative ion permeabilities for NSCCL estimated from the shifts of reversal potential caused by total cation substitution decrease in the order $Cs^+ > Na^+ > Li^+ > Ba^{2+} \geq Sr^{2+} > Ca^{2+} > Mg^{2+}$. NSCCs with more or less similar permeability sequences have been described in other types of smooth muscle cell (Nouailhetas *et al.* 1994; Minami *et al.* 1994; Nakajima *et al.* 1996; Setoguchi *et al.* 1997; Bae *et al.* 1999; Miyoshi *et al.* 2004). Similar permeability sequences have also

been reported for the ligand-gated non-selective cation channels of excitatory synapses, such as the nicotinic acetylcholine receptor channel of the neuromuscular junction (Adams *et al.* 1980), which are generally thought to have a relatively wide pore (see Hille, 2001).

For NSCCS, we have determined the permeability sequence as $Ba^{2+} \geq Sr^{2+} > Ca^{2+} \geq Mg^{2+} > Li^{+} \geq Na^{+} > Cs^{+}$ (see Table 1). NSCCS thus favours the divalent cations including Ca^{2+} for which the permeability ratio is $P_{Ca}/P_{Na} = 2.6$, rather than near 0.3 as in NSCCL. Higher selectivities for divalent over monovalent metal ions have been demonstrated for other smooth muscle NSCCs, such as a noradrenaline-activated NSCC of rabbit portal vein myocytes (Wang & Large, 1991), an ATP-receptor channel of rabbit ear artery myocytes (Benham & Tsien, 1987) and a large conductance Ca^{2+}-activated NSCC of rat portal vein myocytes (Loirand *et al.* 1991). P_{Ca}/P_{Na} ratios greater than 1.0 (between 2 and 90) have also been reported for various types of NSCC functioning as sensory transduction channels, many of which have been suggested to make Ca^{2+} influxes large enough to be physiologically important to the cells expressing them (see pp. 460–462 of Hille, 2001 and references therein). NSCCS may also play an important role as a pathway for Ca^{2+} entry in the ciliary muscle (see below).

Link with muscarinic receptor. It is now generally assumed that the activation of receptor-operated channels by agonists in smooth muscle cells is mediated by pathways coupled with heteromeric GTP-binding proteins (G-proteins). The major G-proteins involved appear to be members of the G_i/G_o subgroup in intestinal and tracheal smooth muscles (Komori *et al.* 1992; Kim *et al.* 1998; Wang & Kotlikoff, 2000). In the present experiments, however, we have observed that the CCh-induced responses of the bovine ciliary muscle are insensitive to pertussis toxin, a specific inactivator of G_i/G_o proteins (Katada & Ui, 1981) as well as to cholera toxin, a specific activator of G-proteins of the G_s class (Hudson & Johnson, 1980). The present observations are consistent with the results of our previous pharmacological experiments (Takai *et al.* 1997) where we examined the effects of relatively selective antagonists and reached the conclusion that the responses of the bovine ciliary muscle to CCh are most likely to be mediated by a muscarinic cholinoceptor of the M_3 subtype (Bonner, 1989), which is usually believed to be coupled with a G-protein of the $G_{q/11}$ class characterized by its insensitivity to the toxins (Pang & Sternweis, 1990; Blank *et al.* 1991; Hepler *et al.* 1993).

Responses accompanied by a clear increase in noise as an indication of the opening of NSCCL are much less frequently evoked by CCh when it is applied in the absence of GTP in the whole-cell recording pipette (present work). Intracellular application of a poorly hydrolysable GTP analogue, GTPγS (Hudson *et al.* 1981), through the pipette makes the turn-on of NSCCL irreversible (see Fig. 9). These observations of the present experiments strongly suggest the involvement of a G-protein-coupled signalling mechanism in the activation of NSCCL. We have shown by the experiments under the on-cell membrane-patch recording configuration that the application of CCh in the pipette, but not its bath application, causes the activation of NSCCL (see Fig. 8). The components of the signalling pathway for NSCCL activation thus appear to be closely associated within a narrow area of the membrane, so that the signal cannot spread beyond the seal of the patch pipette. The first clearly demonstrated example of such a membrane-delimited G-protein-coupled signalling is the activation of $K_{ir3.x}$, a cardiac inwardly rectifying K^+ channel (also called K_{ACh} or GIRK), by acetylcholine (for review, see, e.g. Kurachi, 1995). In this classical example, the response is evoked by the activation of M_2- rather than M_3-muscarinic receptors and the signal is thought to be conveyed through $\beta\gamma$ subunits of G_i to the channel (Reuveny *et al.* 1994; Kofuji *et al.* 1995; Ford *et al.* 1998). Activation of receptor-operated NSCCs by pertussis toxin-sensitive signal transduction mechanisms has also been described in several smooth muscle cells (Inoue & Isenberg, 1990*a*; Komori *et al.* 1992; Wang *et al.* 1997). In these cases, however, it is probably G_α- rather than $G_{\beta\gamma}$-subunits which are involved in the signal transduction. In tracheal (Wang *et al.* 1997) and ileal (Yan *et al.* 2003) smooth muscle cells, the agonist-evoked currents have been shown to be blocked by antibodies specific to $G_{\alpha i}/G_{\alpha o}$ subunits, but not by antibodies to $G_{\alpha q}$ or to $G_{\beta\gamma}$. In contrast to this, in mouse gastric smooth muscle a CCh-evoked NSCC current has been shown to be blocked by $G_{\alpha q/11}$ antibody, whereas it is not affected by $G_{\alpha 0}$ antibody (Lee *et al.* 2003). Experiments using antibodies against G-protein subunits would also be useful to elucidate how NSCCL is linked to M_3 muscarinic receptors by G-proteins.

In contrast to NSCCL, NSCCS tends to be readily activated by CCh even in the absence of GTP in the pipette for whole-cell current recording (see Results). The CCh-evoked response of NSCCS thus appears to be much less dependent on GTP than is that of NSCCL. Presumably the intrinsic production of GTP in most of the ciliary muscle cells under the experimental conditions is insufficient for the activation of NSCCL but is sufficient to allow the passage of the signal from the muscarinic receptor through G-proteins to NSCCS.

If the activation of NSCCS by CCh is to be mediated by a G-protein-coupled pathway, why then does the component of the CCh-evoked response attributable to NSCCS openings quickly disappear after removal of the agonist even in the presence of GTPγS (see Fig. 7*B*)? The present experiments give no clear answer to this question. Several G-proteins of the $G_{q/11}$ class, unlike those of the G_s and G_i classes, are known to display very

low affinity for binding GTPγS under some conditions (Hepler *et al.* 1993). However, the dissociation constant for the interaction of such G-proteins with GTPγS is in the order of 30 μM. With 180–360 μM GTPγS in the pipette even these low affinity G-proteins should be activated almost maximally. Signals from muscarinic receptors might actually reach NSCCS through some novel pathway that is independent of G-proteins.

Inhibition by intracellular Ca^{2+}. In the present experiments we have shown that elevation of the intracellular Ca^{2+} concentration $[Ca^{2+}]_i$ has an inhibitory effect on the CCh-evoked currents (see Fig. 10), confirming our previous observation (Takai *et al.* 1997). The inhibition is especially marked when divalent metal ions are used as the charge carrier. The total amount of the charge during the CCh-evoked response decreases by 90–95% by increasing the $[Ca^{2+}]_i$ from 70 nM to 400 nM, when the extracellular cations were totally replaced with Ba^{2+} or Sr^{2+}, to which NSCCS exhibits relatively high permeabilities. This indicates that the inhibitory effect of Ca^{2+} is particularly strong on NSCCS.

NSCCL appears to be much less susceptible to the inhibition by Ca^{2+}. In our previous experiments (Takai *et al.* 1997), we have shown that CCh can evoke currents with a large noise component even when $[Ca^{2+}]_i$ is increased to 700 nM.

Possible roles for NSCCL and NSCCS in ciliary muscle contraction

In mammalian intestinal smooth muscles, the depolarization resulting from the muscarinic receptor-operated activation of a type of NSCC is thought to trigger Ca^{2+} influx through voltage-gated Ca^{2+} channels, which serve as the main pathway for Ca^{2+} entry during the contraction (Bolton, 1979; Bolton *et al.* 1999). The NSCCs of these muscles, which are strongly activated by elevation of $[Ca^{2+}]_i$, probably function as a component of a positive feedback system to maintain the large Ca^{2+} influx required for strong force generation (Inoue & Isenberg, 1990*a*,*b*). In the ciliary muscle, however, there are several lines of evidence that voltage-gated Ca^{2+} channels make only very little, if any, contribution to the initiation and maintenance of contraction. For example, in bovine and human ciliary muscle bundles it has been shown that contractions induced by a high-K^+ solution (which not only depolarizes the muscle membrane but also causes the release of acetylcholine from the cholinergic nerve terminals) are completely blocked by atropine (Suzuki, 1983). In the dog ciliary muscle, high K^+-induced contraction is also strongly suppressed by atropine although there is a small component which is resistant to atropine and is inhibited by organic Ca^{2+} antagonists (Ito & Yoshitomi, 1986). In a human ciliary muscle cell line, Stahl *et al.* (1992) measured the change of $[Ca^{2+}]_i$ by the fura-2 method. They showed that application of muscarinic agonists resulted in an initial $[Ca^{2+}]_i$ peak followed by a plateau. The initial peak was still clearly observed in the absence of extracellular Ca^{2+} and in the presence of verapamil, whereas the $[Ca^{2+}]_i$ plateau was reversibly abrogated by removal of extracellular Ca^{2+} but was only slightly suppressed by verapamil. Stahl *et al.* (1992) attributed the initial peak to Ca^{2+} release from intracellular stores and the plateau to Ca^{2+} entry through 'receptor-operated' calcium channels.

In the present mechanical experiments on the bovine ciliary muscle bundles, we have observed that removal of Ca^{2+} from the extracellular solution abolishes the tonic phase of the contraction induced by CCh, which is quickly restored by readmisstion of Ca^{2+} (see Fig. 12*A*). This clearly demonstrates the crucial importance of Ca^{2+} influx for sustained contraction of the ciliary muscle. We have then shown that the putative blockers of receptor-operated NSCCs such as SKF96365 (Merritt *et al.* 1990), La^{3+} and Gd^{3+} (Docherty, 1988; Popp *et al.* 1993) dose-dependently inhibit the tonic component of the contraction without strongly affecting the initial phasic component (see Fig. 12*B*). We have also shown by the whole-cell voltage clamp experiments that these agents inhibit, at the same concentrations as those used in the mechanical experiments (Fig. 12*C*), the CCh-evoked NSCCL and NSCCS currents evoked by CCh (see Fig. 11). Moreover, we have demonstrated that the contractile response (Fig. 12*D*) and the whole-cell current response (see Fig. 4*Bb*) induced by CCh exhibit very similar dose dependence. These observations of the present experiments strongly support the notion that either of the two channels serves as a major pathway for the Ca^{2+} entry required for the sustained contraction of the ciliary muscle, which lacks voltage-gated pathways. In the majority of ciliary muscle cells, the current evoked by CCh mainly flows through NSCCS which gives a considerably higher P_{Ca}/P_{Na} ratio than does NSCCL (see above). Therefore, it is probably NSCCS that plays a predominant role in the Ca^{2+} entry under physiological conditions, although NSCCL may also make limited contributions.

Since NSCCS has a very small unitary conductance and is strongly inhibited by elevation of $[Ca^{2+}]_i$ in the working range (see above), a smoothly graded adjustment of $[Ca^{2+}]_i$ will readily be achieved on the basis of an automatic negative feedback mechanism, if a muscarinic stimulation of an appropriate intensity is applied to activate a certain fraction of many copies of NSCCS distributed in the cell membrane. The use of NSCCS as the pathway for Ca^{2+} entry seems to be particularly suitable for the regulation of the ciliary muscle contraction required for fine and stable tuning of the optical focus of the eye.

Possible relationship of the NSCCL and NSCCS to TRPC homologues

The members of the TRPC subfamily of TRP channels have been receiving increasing attention as molecular candidates for receptor-operated NSCCs in various tissues including smooth muscles (see Clapham *et al.* 2001; Minke & Cook, 2002; Inoue *et al.* 2003). For example, Inoue *et al.* (2001) have recently shown that heterologous expression of murine TRPC6 in HEK293 cells reproduces the biophysical and pharmacological properties of α_1-adrenoceptor-activated NSCCs very well, previously identified in smooth muscle of rabbit portal vein. More recently, Lee *et al.* (2003) have found close similarities between the currents observed in HEK293 cells transfected with a TRPC5 expression vector and the NSCC currents activated by muscarinic stimulation in smooth muscle cells of the murine stomach.

The present RT-PCR experiments have demonstrated the existence of at least four types (TRPC1, TRPC3, TRPC4 and TRPC6) of TRP mRNA in the bovine ciliary muscle (whole tissue). It seems unlikely from the comparison of channel properties, as shown in Table 3, that NSCCL and/or NSCCS could be simply a single type of TRPC. However, evidence is accumulating that several TRPC homologues can bind together to form heteromeric oligomers which are drastically different from their homomeric oligomers in critical electrophysiological properties such as unitary conductance, ion selectivity, voltage dependence and Ca^{2+} sensitivity (Lintschinger *et al.* 2000; Strübing *et al.* 2001). It would be highly interesting to examine whether NSCCL and NSCCS are molecular correlates of some types of heteromeric oligomer of the TRP homologues.

References

Adams DJ, Dwyer TM & Hille B (1980). The permeability of endplate channels to monovalent and divalent metal cations. *J Gen Physiol* **75**, 493–510.

Albert AP & Large WA (2002). A Ca^{2+}-permeable non-selective cation channel activated by depletion of internal Ca^{2+} stores in single rabbit portal vein myocytes. *J Physiol* **538**, 717–728.

Amédée T, Benham CD, Bolton TB, Byrne NG & Large WA (1990). Potassium, chloride and non-selective cation conductances opened by noradrenaline in rabbit ear artery cells. *J Physiol* **423**, 551–568.

Ashoori F, Takai A & Tomita T (1985). The response of non-pregnant rat myometrium to oxytocin in Ca-free solution. *Br J Pharmacol* **84**, 175–183.

Bae YM, Park MK, Lee SH, Ho WK & Earm YE (1999). Contribution of Ca^{2+}-activated K^+ channels and non-selective cation channels to membrane potential of pulmonary arterial smooth muscle cells of the rabbit. *J Physiol* **514**, 747–758.

Benham CD & Tsien RW (1987). A novel receptor-operated Ca^{2+}-permeable channel activated by ATP in smooth muscle. *Nature* **328**, 275–278.

Blank JL, Ross AH & Exton JH (1991). Purification and characterization of two G-proteins that activate the β_1 isozyme of phosphoinositide-specific phospholipase C. Identification as members of the G_q class. *J Biol Chem* **266**, 18206–18216.

Bolton TB (1979). Mechanisms of action of transmitters and other substances on smooth muscle. *Physiol Rev* **59**, 606–718.

Bolton TB, Prestwich SA, Zholos AV & Gordienko DV (1999). Excitation-contraction coupling in gastrointestinal and other smooth muscles. *Annu Rev Physiol* **61**, 85–115.

Bonner TI (1989). The molecular basis of muscarinic receptor diversity. *Trends Neurosci* **12**, 148–151.

Clapham DE, Runnels LW & Strübing C (2001). The TRP ion channel family. *Nat Rev Neurosci* **2**, 387–396.

Colquhoun D & Hawkes AG (1977). Relaxation and fluctuations of membrane currents that flow through drug-operated channels. *Proc R Soc Lond B Biol Sci* **199**, 231–262.

Cull-Candy SG, Howe JR & Ogden DC (1988). Noise and single channels activated by excitatory amino acids in rat cerebellar granule neurones. *J Physiol* **400**, 189–222.

Dickinson KE, Frizzell RA & Sekar MC (1992). Activation of T84 cell chloride channels by carbachol involves a phosphoinositide-coupled muscarinic M_3 receptor. *Eur J Pharmacol* **225**, 291–298.

Docherty RJ (1988). Gadolinium selectively blocks a component of calcium current in rodent neuroblastoma × glioma hybrid (NG108-15) cells. *J Physiol* **398**, 33–47.

Ford CE, Skiba NP, Bae H, Daaka Y, Reuveny E, Shekter LR, Rosal R, Weng G, Yang CS, Iyengar R, Miller RJ, Jan LY, Lefkowitz RJ & Hamm HE (1998). Molecular basis for interactions of G protein $\beta\gamma$ subunits with effectors. *Science* **280**, 1271–1274.

Freichel M, Suh SH, Pfeifer A, Schweig U, Trost C, Weissgerber P, Biel M, Philipp S, Freise D, Droogmans G, Hofmann F, Flockerzi V & Nilius B (2001). Lack of an endothelial store-operated Ca^{2+} current impairs agonist-dependent vasorelaxation in TRP4–/– mice. *Nat Cell Biol* **3**, 121–127.

Friel DD (1988). An ATP-sensitive conductance in single smooth muscle cells from the rat vas deferens. *J Physiol* **401**, 361–380.

Galvez A, Gimenez Gallego G, Reuben JP, Roy Contancin L, Feigenbaum P, Kaczorowski GJ & Garcia ML (1990). Purification and characterization of a unique, potent, peptidyl probe for the high conductance calcium-activated potassium channel from venom of the scorpion *Buthus tamulus*. *J Biol Chem* **265**, 11083–11090.

Glasser A & Kaufman PL (2003). Accommodation and presbyopia. In *Adler's Physiology of the Eye: Clinical Application*, ed. Kaufman PL & Alm A, pp. 197–233. Mosby, St Louis.

Golovina VA, Platoshyn O, Bailey CL, Wang J, Limsuwan A, Sweeney M, Rubin LJ & Yuan JX (2001). Upregulated TRP and enhanced capacitative Ca^{2+} entry in human pulmonary artery myocytes during proliferation. *Am J Physiol Heart Circ Physiol* **280**, H746–H755.

Hepler JR, Kozasa T, Smrcka AV, Simon MI, Rhee SG, Sternweis PC & Gilman AG (1993). Purification from Sf9 cells and characterization of recombinant $G_{q\alpha}$ and $G_{11\alpha}$: activation of purified phospholipase C by G_α subunits. *J Biol Chem* **268**, 14367–14375.

Hille B (2001). *Ion Channels of Excitable Membranes*, 3rd edn. Sinauer Associates, Inc, Sunderland, MA, USA.

Hoffmann HM & Dionne VE (1983). Temperature dependence of ion permeation at the endplate channel. *J Gen Physiol* **81**, 687–703.

Hofmann T, Obukhov AG, Schaefer M, Harteneck C, Gudermann T & Schultz G (1999). Direct activation of human TRPC6 and TRPC3 channels by diacylglycerol. *Nature* **397**, 259–263.

Howe JR, Colquhoun D & Cull-Candy SG (1988). On the kinetics of large-conductance glutamate-receptor ion channels in rat cerebellar granule neurons. *Proc R Soc Lond B Biol Sci* **233**, 407–422.

Hudson TH & Johnson GL (1980). Peptide mapping of adenylate cyclase regulatory proteins that are cholera toxin substrates. *J Biol Chem* **255**, 7480–7486.

Hudson TH, Roeber JF & Johnson GL (1981). Conformational changes of adenylate cyclase regulatory proteins mediated by guanine nucleotides. *J Biol Chem* **256**, 1459–1465.

Inoue R, Hanano T, Shi J, Mori Y & Ito Y (2003). Transient receptor potential protein as a novel non-voltage-gated Ca^{2+} entry channel involved in diverse pathophysiological functions. *J Pharmacol Sci* **91**, 271–276.

Inoue R & Isenberg G (1990*a*). Acetylcholine activates nonselective cation channels in guinea pig ileum through a G protein. *Am J Physiol* **258**, C1173–C1178.

Inoue R & Isenberg G (1990*b*). Intracellular calcium ions modulate acetylcholine-induced inward current in guinea-pig ileum. *J Physiol* **424**, 73–92.

Inoue R, Kitamura K & Kuriyama H (1987). Acetylcholine activates single sodium channels in smooth muscle cells. *Pflugers Arch* **410**, 69–74.

Inoue R & Kuriyama H (1993). Dual regulation of cation-selective channels by muscarinic and alpha 1-adrenergic receptors in the rabbit portal vein. *J Physiol* **465**, 427–448.

Inoue R, Okada T, Onoue H, Hara Y, Shimizu S, Naitoh S, Ito Y & Mori Y (2001). The transient receptor potential protein homologue TRP6 is the essential component of vascular α_1-adrenoceptor-activated Ca^{2+}-permeable cation channel. *Circ Res* **88**, 325–332.

Ito Y & Yoshitomi T (1986). Membrane and contractile properties of the dog ciliary muscle. *Br J Pharmacol* **88**, 629–638.

Janssen LJ & Sims SM (1992). Acetylcholine activates non-selective cation and chloride conductances in canine and guinea-pig tracheal myocytes. *J Physiol* **453**, 197–218.

Kamouchi M, Philipp S, Flockerzi V, Wissenbach U, Mamin A, Raeymaekers L, Eggermont J, Droogmans G & Nilius B (1999). Properties of heterologously expressed hTRP3 channels in bovine pulmonary artery endothelial cells. *J Physiol* **518**, 345–358. Erratum: *J Physiol* **519**, 923.

Katada T & Ui M (1981). Islet-activating protein: a modifier of receptor-mediated regulation of rat islet adenylate cyclase. *J Biol Chem* **256**, 8310–8317.

Kim YC, Kim SJ, Sim JH, Cho CH, Juhnn YS, Suh SH, So I & Kim KW (1998). Suppression of the carbachol-activated nonselective cationic current by antibody against alpha subunit of G_o protein in guinea-pig gastric myocytes. *Pflugers Arch* **436**, 494–496.

Kofuji P, Davidson N & Lester HA (1995). Evidence that neuronal G-protein-gated inwardly rectifying K^+ channels are activated by $G_{\beta\gamma}$ subunits and function as heteromultimers. *Proc Natl Acad Sci U S A* **92**, 6542–6546.

Komori S, Kawai M, Takewaki T & Ohashi H (1992). GTP-binding protein involvement in membrane currents evoked by carbachol and histamine in guinea-pig ileal muscle. *J Physiol* **450**, 105–126.

Konno F & Takayanagi I (1985). Muscarinic acetylcholine receptors in the rabbit ciliary body smooth muscle: spare receptors and threshold phenomenon. *Jpn J Pharmacol* **38**, 91–99.

Korbmacher C, Helbig H, Coroneo M, Erickson Lamy KA, Stiemer B, Tamm E, Lütjen Drecoll E & Wiederholt M (1990). Membrane voltage recordings in a cell line derived from human ciliary muscle. *Invest Ophthalmol Vis Sci* **31**, 2420–2430.

Kurachi Y (1995). G protein regulation of cardiac muscarinic potassium channel. *Am J Physiol* **269**, C821–C830.

Lee YM, Kim BJ, Kim HJ, Yang DK, Zhu MH, Lee KP, So I & Kim KW (2003). TRPC5 as a candidate for the nonselective cation channel activated by muscarinic stimulation in murine stomach. *Am J Physiol Gastrointest Liver Physiol* **284**, G604–G616.

Lewis CA (1979). Ion-concentration dependence of the reversal potential and the single channel conductance of ion channels at the frog neuromuscular junction. *J Physiol* **286**, 417–445.

Lintschinger B, Balzer-Geldsetzer M, Baskaran T, Graier WF, Romanin C, Zhu MX & Groschner K (2000). Coassembly of Trp1 and Trp3 proteins generates diacylglycerol- and Ca^{2+}-sensitive cation channels. *J Biol Chem* **275**, 27799–27805.

Loirand G, Pacaud P, Baron A, Mironneau C & Mironneau J (1991). Large conductance calcium-activated non-selective cation channel in smooth muscle cells isolated from rat portal vein. *J Physiol* **437**, 461–475.

McFadzean I & Gibson A (2002). The developing relationship between receptor-operated and store-operated calcium channels in smooth muscle. *Br J Pharmacol* **135**, 1–13.

Mahler HR & Cordes EH (1969). *Biological Chemistry*, 2nd edn. Harper & Row Publishers, New York.

Merritt JE, Armstrong WP, Benham CD, Hallam TJ, Jacob R, Jaxa-Chamiec A, Leigh BK, McCarthy SA, Moores KE & Rink TJ (1990). SK&F 96365, a novel inhibitor of receptor-mediated calcium entry. *Biochem J* **271**, 515–522.

Minami K, Fukuzawa K & Inoue I (1994). Regulation of a non-selective cation channel of cultured porcine coronary artery smooth muscle cells by tyrosine kinase. *Pflugers Arch* **426**, 254–257.

Minke B & Cook B (2002). TRP channel proteins and signal transduction. *Physiol Rev* **82**, 429–472.

Miyoshi H, Yamaoka K, Garfield RE & Ohama K (2004). Identification of a non-selective cation channel current in myometrial cells isolated from pregnant rats. *Pflugers Arch* **447**, 457–464.

Nakajima T, Hazama H, Hamada E, Wu SN, Igarashi K, Yamashita T, Seyama Y, Omata M & Kurachi Y (1996). Endothelin-1 and vasopressin activate Ca^{2+}-permeable non-selective cation channels in aortic smooth muscle cells: mechanism of receptor-mediated Ca^{2+} influx. *J Mol Cell Cardiol* **28**, 707–722.

Nouailhetas VL, Aboulafia J, Frediani Neto E, Ferreira AT & Paiva AC (1994). A Na^{+}-sensitive cation channel modulated by angiotensin II in cultured intestinal myocytes. *Am J Physiol* **266**, C1538–C1543.

Pang IH & Sternweis PC (1990). Purification of unique α subunits of GTP-binding regulatory proteins (G proteins) by affinity chromatography with immobilized $\beta\gamma$ subunits. *J Biol Chem* **265**, 18707–18712.

Philipp S, Cavalie A, Freichel M, Wissenbach U, Zimmer S, Trost C, Marquart A, Murakami M & Flockerzi V (1996). A mammalian capacitative calcium entry channel homologous to Drosophila TRP and TRPL. *EMBO J* **15**, 6166–6171.

Popp R, Englert HC, Lang HJ & Gögelein H (1993). Inhibitors of nonselective cation channels in cells of the blood–brain barrier. *EXS* **66**, 213–218.

Reuveny E, Slesinger PA, Inglese J, Morales JM, Iniguez-Lluhi JA, Lefkowitz RJ, Bourne HR, Jan YN & Jan LY (1994). Activation of the cloned muscarinic potassium channel by G protein $\beta\gamma$ subunits. *Nature* **370**, 143–146.

Schaefer M, Plant TD, Obukhov AG, Hofmann T, Gudermann T & Schultz G (2000). Receptor-mediated regulation of the nonselective cation channels TRPC4 and TRPC5. *J Biol Chem* **275**, 17517–17526.

Setoguchi M, Ohya Y, Abe I & Fujishima M (1997). Stretch-activated whole-cell currents in smooth muscle cells from mesenteric resistance artery of guinea-pig. *J Physiol* **501**, 343–353.

Sigworth FJ (1980). The variance of sodium current fluctuations at the node of Ranvier. *J Physiol* **307**, 97–129.

Snedecor GW & Cochran WG (1980). *Statistical Methods*, 7th edn. Iowa State University Press, Ames, IA, USA.

Stahl F, Gebauer B, Lepple Wienhues A, Langenbeck Groh G, Berweck S & Wiederholt M (1992). Characterization of acetylcholine- and endothelin-induced calcium entry in cultured human ciliary muscle cells. *Pflugers Arch* **422**, 105–111.

Strübing C, Krapivinsky G, Krapivinsky L & Clapham DE (2001). TRPC1 and TRPC5 form a novel cation channel in mammalian brain. *Neuron* **29**, 645–655.

Suzuki R (1983). Neuronal influence on the mechanical activity of the ciliary muscle. *Br J Pharmacol* **78**, 591–597.

Takai Y, Awaya S & Takai A (1997). Activation of non-selective cation conductance by carbachol in freshly isolated bovine ciliary muscle cells. *Pflugers Arch* **433**, 705–712.

Trepakova ES, Csutora P, Hunton DL, Marchase RB, Cohen RA & Bolotina VM (2000). Calcium influx factor directly activates store-operated cation channels in vascular smooth muscle cells. *J Biol Chem* **275**, 26158–26163.

Trepakova ES, Gericke M, Hirakawa Y, Weisbrod RM, Cohen RA & Bolotina VM (2001). Properties of a native cation channel activated by Ca^{2+} store depletion in vascular smooth muscle cells. *J Biol Chem* **276**, 7782–7790.

Wang YX, Fleischmann BK & Kotlikoff MI (1997). M_2 receptor activation of nonselective cation channels in smooth muscle cells: calcium and G_i/G_o requirements. *Am J Physiol* **273**, C500–C508.

Wang Q, Hogg RC & Large WA (1993). A monovalent ion-selective cation current activated by noradrenaline in smooth muscle cells of rabbit ear artery. *Pflugers Arch* **423**, 28–33.

Wang YX & Kotlikoff MI (2000). Signalling pathway for histamine activation of non-selective cation channels in equine tracheal myocytes. *J Physiol* **523**, 131–138.

Wang Q & Large WA (1991). Noradrenaline-evoked cation conductance recorded with the nystatin whole-cell method in rabbit portal vein cells. *J Physiol* **435**, 21–39.

Yan HD, Okamoto H, Unno T, Tsytsyura YD, Prestwich SA, Komori S, Zholos AV & Bolton TB (2003). Effects of G-protein-specific antibodies and $G_{\beta\gamma}$ subunits on the muscarinic receptor-operated cation current in guinea-pig ileal smooth muscle cells. *Br J Pharmacol* **139**, 605–615.

Zitt C, Obukhov AG, Strübing C, Zobel A, Kalkbrenner F, Lückhoff A & Schultz G (1997). Expression of TRPC3 in Chinese hamster ovary cells results in calcium-activated cation currents not related to store depletion. *J Cell Biol* **138**, 1333–1341.

Zitt C, Zobel A, Obukhov AG, Harteneck C, Kalkbrenner F, Lückhoff A & Schultz G (1996). Cloning and functional expression of a human Ca^{2+}-permeable cation channel activated by calcium store depletion. *Neuron* **16**, 1189–1196.

Acknowledgements

This work was partly supported by Grants-in-Aid from the Ministry of Education, Culture, Sports, Science and Technology of Japan (nos 13470365 and 15659407) to A.T. We thank Dr Peter G. Osborne of our laboratory for valuable comments.